



Deliverable 16.8: MAGIC - T1 - S/T 4-1 – 4/2
Chemo-mechanical numerical coupling development
and up-scaling methods

Work Package 16



This project has received funding from the European Union's Horizon 2020 research and innovation programme 2014-2018 under grant agreement N°847593.



EURAD Deliverable 16.8 – MAGIC - S/T 4-1 – 4/2 -Chemo-mechanical numerical coupling development and up-scaling methods

Document information

Project Acronym	EURAD
Project Title	European Joint Programme on Radioactive Waste Management
Project Type	European Joint Programme (EJP)
EC grant agreement No.	847593
Project starting / end date	1st June 2019 – 30 May 2024
Work Package No.	16
Work Package Title	Chemo-Mechanical AGIng of Cementitious materials
Work Package Acronym	MAGIC
Deliverable No.	16.8
Deliverable Title	Chemo-mechanical numerical coupling development and up-scaling methods
Lead Beneficiary	JUELICH (UFZ)
Contractual Delivery Date	February 2023
Actual Delivery Date	April 2024
Type	Report
Dissemination level	PU
Authors	Vanessa Montoya (UFZ; SCK-CEN), Mostafa Mollaali (UFZ), Alain Sellier (LMDC), Laurie Lacarrière (LMDC), Layla Ibrahim (LMDC), Nicolas Seigneur (Mines Paris Tech), Stéphane Poyet (CEA), Benoît Bary (CEA), Victor Vilarrasa (CSIC), Sebastian Ignacio Gonzalez Fuentes (CSIC), Jianfu Shao (LAMCUBE), Keita Yoshioka (UFZ; Montanuniversität Leoben), Olaf Kolditz (UFZ), Sergey Churakov (PSI), Athanasios Mokos (PSI)

To be cited as:

Montoya, V; Mollaali, M; Sellier, A; Lacarrière, L; Ibrahim, L; Seigneur, N; Poyet, S; Bary, B; Vilarrasa, V; Gonzalez Fuentes, S; Shao, J; Yoshioka, K; Churakov, S; Kolditz, O ; Mokos, A (Dauzères et al.): S/T 4-1 – 4/2 -Chemo-mechanical numerical coupling development and up-scaling methods. Final version as of 04.04.2024 of deliverable D16.8 of the HORIZON 2020 project EURAD. EC Grant agreement no: 847593.

Disclaimer

All information in this document is provided "as is" and no guarantee or warranty is given that the information is fit for any particular purpose. The user, therefore, uses the information at its sole risk and liability. For the avoidance of all doubts, the European Commission or the individual Colleges of EURAD (and their participating members) has no liability in respect of this document, which is merely representing the authors' view.

Acknowledgement

This document is a deliverable of the European Joint Programme on Radioactive Waste Management (Dauzères et al.). EURAD has received funding from the European Union's Horizon 2020 research and innovation programme under grant agreement No 847593.

Status of deliverable		
	By	Date
Delivered (Lead Beneficiary)	Vanessa Montoya (UFZ; SCK-CEN) Mostafa Mollaali, Olaf Kolditz (UFZ)	10/2023 Revised version 12/2023
Verified (WP Leader)	Alexandre Dauzères (IRSN)	10/2023 – 014/2024
Reviewed (Reviewers)	Board members	10/2023 – 01/2024
Approved (PMO)	Bernd Grambow	04/2024
Submitted to EC (Coordinator)	Andra (Coordinator)	04/2024

Executive Summary

The objective of this report is to summarise the modelling work of the MAGIC WP and to establish a permanent reference chemo-mechanical model for the deterioration of both Portland and low pH concretes in relevant repository environments, taking into account representative boundary conditions. The report focuses on Task 4 and in particular on the development of chemomechanical numerical coupling and up-scaling methods. The collaboration between participants from different organisations and institutions has resulted in a comprehensive review of chemomechanical numerical coupling and upscaling of mechanical properties related to cement alteration.

The report is divided into two main sections. The first section summarises the model approaches (at different scales) and the chemo-mechanical numerical coupling schemes of PSI, LMDC, UFZ, CEA/Mines PSL. The second section deals with upscaling approaches for chemomechanical processes from aggregates to near-field processes in order to combine pore to macroscale models. The focus of deliverable D16.8 is to summarise the modelling approaches and provide results for benchmarks. The following deliverable D16.9 will present application results for the reference model.

The key results from our research include:

PSI (Section 1.1) presents their pore scale approach to modelling chemical reactions based on Lattice Boltzmann methods. They simulate Ca leaching at the pore scale, taking into account the dissolution of portlandite as the pore solution (OPA) enters the concrete. They successfully use surrogate models based on artificial neural networks to speed up the computationally expensive simulations. The surrogate models are trained using the GEM reaction code.

LMDC (section 1.2) introduces the finite element approach for macroscale modelling of chemomechanical processes under water-saturated conditions. The model fundamentals are presented, including the required constitutive relationships of the chemical reactions involved in cement degradation. The focus is on reactive transport processes, mechanical processes are not considered. The model results are presented in D16.9.

The UFZ (section 1.3) presents a hydro-chemical-mechanical coupled model by combining OpenGeoSys (OGS) and PHREEQC, which allows a high flexibility to include different chemical reactions. OGS uses the finite element method in combination with variational phase fields. The functionality of the model has been demonstrated with a benchmark study including fracture initiation and propagation by tensile stresses and calcite dissolution within the fracture by pore water attack.

CEA/Mines Paris Tech (Section 1.4) presents a conceptual thermo-hydro-mechanical-chemical model for unsaturated conditions. A multi-continua approach is preferred to represent fractured porous media. A code coupling of CAST3M (damage processes) and HYTEC (reactive transport) is used. As a test example, the representation of accelerated carbonation and related damage processes (microcracking) in cementitious material is presented.

The second section deals with upscaling methods of mechanical properties and cement alteration:

LAMCUBE (section 2.1) presents an upscaling approach by homogenisation method from micro to macro scale with an intermediate mesoscopic step to represent the aggregates of the cement matrix. Effective properties are derived by analytical averaging methods. In addition, artificial neural networks (ANNs) are used to predict the effective elastic properties of concrete. An important parameter of the chemomechanical processes is the fracture strength, which has also been estimated by ANNs.

Finally, CSIC (section 2.2) introduces a chemo-mechanical coupling approach by combining CODE_BRIGHT (HM processes) and Retraso (reactive transport of solutes). A test case representing a tunnel section with an altered concrete zone has been introduced. A stress path analysis was performed on the mechanical model. Model results for chemo-mechanical processes are presented in D16.9.

Table of content

Executive Summary.....	4
Table of content.....	5
List of figures	6
List of Tables	8
Glossary.....	9
General introduction	12
1. Chemo-mechanical numerical coupling	14
1.1 Pore-scale model implementation (led by PSI)	14
1.2 Chemo-mechanical models in saturated environment (led by LMDC).....	17
1.2.1 Strategy for model reduction	18
1.2.2 Model implementation.....	23
1.3 Fracture formation and propagation models (led by UFZ)	24
1.3.1 Coupled processes	24
1.3.2 The influence of the phase field and changes in porosity on the coupling process	26
1.3.3 Preliminary results	27
1.4 Damage model in unsaturated conditions (led by CEA/Mines PSL)	29
1.4.1 Context and approach description.....	29
1.4.2 Methodology	29
1.4.3 Results.....	30
1.4.4 Perspectives	32
2. Upscaling of mechanical properties vs cement alteration	33
2.1 Analytical homogenization (led by LAMCUBE)	33
2.1.1 Simplified micro-structure considered	33
2.1.2 Chemical mechanical coupling.....	33
2.1.3 Elastic properties	33
2.1.4 Failure strength.....	38
2.2 Other upscaling methods (led by CSIC).....	39
2.2.1 Introduction	39
2.2.2 Hydro-Mechanical model.....	40
2.2.3 Chemical modelling	44
REFERENCES	48

List of figures

Figure 1.1-1 Comprehensive Overview of the Workflow for Task 4.....	12
Figure 1.1-2: Ca leaching LB simulations, considering the dissolution of portlandite. The left column shows the initial state, while the right shows the state after 1.5 million LB steps. Red nodes signify correctly dissolving portlandite, white nodes are inactive portlandite not in contact with liquid, light blue signify inactive CSH and aggregates and dark blue is water. a) and b) show the full 3D microstructure, c) and d) show a 2D slice at 30 μm from the edge and e) and f) show a 2D slice at 60 μm from the edge	16
Figure 1.2-1: Service life of the disposal structure	17
Figure 1.2-2: Global approach scheme	17
Figure 1.2-3 Thermodynamic equilibrium curve at 25°C (Gerard, Pijaudier-Cabot, & Laborderie, 1998)	19
Figure 1.2-4 Effect of temperatures on the equilibrium curve (Peycelon, Blanc, & Mazoin, 2006).....	19
Figure 1.2-5 : Elementary equilibrium curve for the portlandite	20
Figure 1.2-6 Effect of temperature on the equilibrium curve of the portlandite.	21
Figure 1.2-7 Algorithm of resolution.	23
Figure 1.3-1 Fully coupled chemo-hydro-mechanical variational phase field model.	25
Figure 1.3-2 Schematic view a fully couple benchmark.	27
Figure 1.3-3 Profiles of calcite (top left), porosity (top right), displacement (bottom left), and phase field (bottom right) before fracture propagation.....	28
Figure 1.3-4 Profiles of calcite (top left), porosity (top right), displacement (bottom left), and phase field (bottom right) after fracture propagation.....	28
Figure 1.4-1: Illustration of the approach.....	29
Figure 1.4-2 Mineralogical spatial maps after 40, 160 and 326 days of accelerated carbonation of the C ₃ S paste.....	31
Figure 1.4-3 Mechanical spatial maps after 40, 160 and 326 days of accelerated carbonation of the C ₃ S paste.	32
Figure 2.1-1 REV of concretes with pores and aggregates.	33
Figure 2.1-2 Variation of relative elastic modulus κ_{hom}/κ_s and μ_{hom}/μ_s with inclusion volume fraction and porosity for concrete materials.	35
Figure 2.1-3 Artificial neural network structure for predicting effective elastic properties of concrete. .	36
Figure 2.1-4 Variations of normalized effective elastic moduli with porosity or inclusion fraction for different values of κ_i/κ_s and μ_i/μ_s for concrete materials.	38
Figure 2.1-5 A BP neural network model to evaluate the microscopic parameter of concrete materials.	39
Figure 2.1-6 Correlation between predicted and exact values of T' and h'.	39
Figure 2.2-1: 2D HM model dimensions.	41
Figure 2.2-2: Analysed points.....	42
Figure 2.2-3: Stress path of concrete in the analysed points.	43
Figure 2.2-4: Stress path of rock analysed points.....	44

List of Tables

Table 1.2-1 variables of the chemical degradation model of the cement paste.....	18
Table 2.2-1 Material properties (HM process).....	42
Table 2.2-2: Initial composition of concrete and rock for calculations.....	46
Table 2.2-3 Initial composition (total molalities) of concrete and rock porewaters. Equilibrium and charge balance constraints are indicated in parentheses.....	47

Glossary

AAR	Alkali aggregate reactions
ANN	Artificial neural networks
ASR	Alkali silica reactions
ASTM	American Society for Testing and Materials
ATP	Adenosine Triphosphate
BSA	Biogenic sulphuric acid
CASH	Calcium Aluminate silicate Hydrates
CDF	Cumulative Distribution Function
CEBAMA	Cement Based Materials
CEM	Cement (CEM I, CEM II...)
CFL	Courant-Friedrichs-Lewy
CH	Calcium hydroxide: Portlandite
CI	Cement-clay Interaction
CIGEO	Industrial Centre for Geological Disposal
CKD	Cement kiln dust
CNT	Classical Nucleation Theory
CORI	Cement Organic Radionuclide Interactions
COX	Callovo-Oxfordian clay
CSH	Calcium Silicates Hydrates
DDL	Diffuse double layer
DEM	Discrete Element Method
EC	European Commission
EDS	Energy dispersive spectroscopy
EPS	Extracellular Polymeric Substances
EPS	Extracellular polymeric substances
ESEM	Environmental Scanning Electron Microscopy
EU	European Union
EURAD	European Joint Programme on Radioactive Waste Management
FDM	Finite difference method
FE	Finite Element

EURAD Deliverable 16.8 – MAGIC - S/T 4-1 – 4/2 -Chemo-mechanical numerical coupling development and up-scaling methods

FEM	Finite Element Method
FFT	Fast fourier transform
GC	Gouy-Chapman (model)
GDF	Geological disposal facilities
GEM	Gibbs Energy Minimization
HET	Heterogeneous
HLW	High-level waste
HON	Homogeneous
HPF	Hyperalkaline Plume in Fractured Rock
ILW	Intermediate level waste
ISA	Iso-Saccharinic Acid
ITZ	Interfacial Transtion zone
LAC	Low Alkaline Cement
LB	Lattice Boltzmann (method)
LBM	Lattice Boltzman Modelling
LCS	Long -term cement studies project
LLW	Low level waste
LMA	Law of Mass Action
MAGIC	The chemo-mechanical aging of cementitious materials
MGC	Modified Gouy Chapman model
MICP	Microbial induced calcite precipitation
MS	Member states
MSH	Magnesium silicate hydrate
NRUS	Nonlinear Resonant Ultrasound Spectroscopy
NS	Navier-Stokes
OPA	Opalinus clay
OPC	Ordinary Portland Cement
PB	Poisson Boltzmann
PDF	Probability density function
R&D	Research and Development
REV	Representative Elementary Volume
RH	Relative humidity
RUS	Resonant Ultrasound Spectroscopy

EURAD Deliverable 16.8 – MAGIC - S/T 4-1 – 4/2 -Chemo-mechanical numerical coupling development and up-scaling methods

SEM	Scanning Electron Microscope
SNT	Supersaturation-Nucleation-Time
SOB	Sulphur-oxidizing bacteria
SOTA	State of the art
SRB	Sulfate reducing bacteria
THM	Thermo-hydro-mechanical
URL	Underground Rock Laboratory
VFA	Volatil fatty acids
XAS	X-ray absorbtion spectroscopy
XRD	X-ray diffraction analysis

General introduction

MAGIC, which stands for Multi-scale Analysis of the Chemo-mechanical Evolution of Cementitious Materials in Geological Disposal Environments, has several key objectives. Firstly, it seeks to understand and quantify how cementitious materials, like concrete, evolve chemically and mechanically over different scales when exposed to the chemical degradation expected in repository environments. This involves identifying the primary chemical reactions that occur during the re-saturation phase and under saturated conditions at the repository scale. Additionally, MAGIC aims to create a fundamental chemo-mechanical model for both Portland and low-pH concretes, considering realistic disposal conditions. Lastly, it aims to assess the impact of microbial activity on cementitious materials properties in partially and fully saturated conditions.

The motivation behind these goals arises from significant knowledge gaps in the field. Most existing experimental data focuses on short-term material evolution, leaving the long-term mechanical integrity of cementitious materials largely unknown. MAGIC aims to address critical questions, such as how various chemical degradation processes affect the mechanical properties of these materials and whether microbial activity plays a role in altering the expected chemical evolution. Moreover, it seeks to develop models that can predict the long-term mechanical behaviour of cementitious materials during hydraulic transients or under fully saturated conditions, taking into account both chemical evolution and microbial activity. Ultimately, MAGIC aims to provide a comprehensive and multi-scale understanding of these complex processes in cementitious materials.

This deliverable focused on task 4 activities, has a clear objective: it aims to establish long-term reference chemo-mechanical models for the degradation of both Portland and low-pH concretes in relevant disposal environments while taking into account representative boundary conditions.

The structure of Task 4 workflow as well as corresponding collaborations are depicted in Figure 1.1-1.

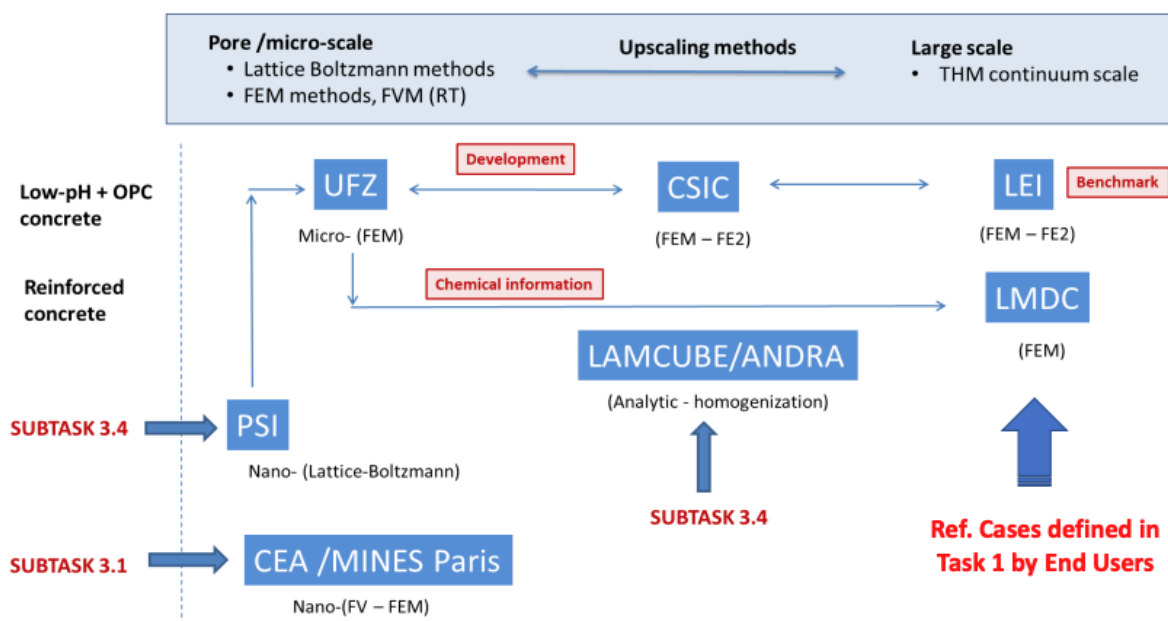


Figure 1.1-1 Comprehensive Overview of the Workflow for Task 4

EURAD Deliverable 16.8 – MAGIC - S/T 4-1 – 4/2 -Chemo-mechanical numerical coupling development and up-scaling methods

The expected outcomes from this effort include several key components. Firstly, it seeks to compile a comprehensive multiscale experimental dataset that connects the chemical degradation, occurring in conjunction with various disturbances, to mechanical parameters such as compressive and tensile strengths, Young's modulus evolution, and the formation and dynamics of cracks. Secondly, the project aims to pinpoint the primary reactive mechanisms at play and understand their implications for the mechanical behaviour of both low-pH and Portland cementitious materials. Thirdly, it plans to develop models that describe how mechanical behaviour changes as a result of chemical evolution at the experimental scale. Additionally, it intends to establish a law for the mechanical behaviour of the materials, considering the competing chemical and hydrodynamical processes occurring at different scales. Lastly, task 4.3 treats the long-term mechanical evolution of concrete structures when exposed to disposal conditions, taking into consideration chemical disturbances.

1. Chemo-mechanical numerical coupling

1.1 Pore-scale model implementation (led by PSI)

Cementitious materials are hierarchical porous media with characteristic microstructure features controlling transport phenomena and reactivity at different scales (Dauzères et al., 2022). Pore size distribution in cement range from few nanometres (cement gel pores) to few millimetres (macroscopic cement pores) (Gong, Zhang, Sicat, & Ueda, 2014; R. A. Patel et al., 2018). The complexity is compounded by various chemical processes such as carbonation (Dauzères et al., 2022; Y. Huang, Shao, Wieland, Kolditz, & Kosakowski, 2018; Phung et al., 2016; von Greve-Dierfeld et al., 2020), interaction with other materials (for example host clay for radioactive waste repositories (Savage & Cloet, 2018) or aggressive species ingressions such as sulphate (Dauzères, 2016; Schmidt, Lothenbach, Romer, Neuenschwander, & Scrivener, 2009) or the presence of microbial micro-organisms (De Graef et al., 2005). These interactions lead to non-linear changes in the porosity and the chemical structure of cement (Barbara Lothenbach & Winnefeld, 2006; Mäder et al., 2018), occurring across different spatial and temporal scales.

In particular, small changes in the pore connectivity and preferential transport pathways can result in substantial alteration of macroscopic transport properties of the materials, such as the permeability and diffusivity. To simulate such processes accurately, a multi-scale approach, operating on both the continuum and the pore-scale is required (Churakov & Prasianakis, 2018). The focus in this section is on the pore-level with the Lattice-Boltzmann (Bilke et al.) method selected for the fluid simulation due to its versatility at the mesoscale and the possibility to simulate in 3D the evolution of the microstructure (H. Huang, Sukop, & Lu, 2015; Prasianakis, Curti, Kosakowski, Poonosamy, & Churakov, 2017; Prasianakis, Gatschet, Abbasi, & Churakov, 2018). The LB method is based on the solution of the kinetic Boltzmann equation, which at the macroscopic limit recovers the Navier-Stokes equations (Lallemand & Luo, 2000; Qian, d'Humières, & Lallemand, 1992). The lattice can then simulate complex interfacial fluid-solid interactions by adapting its nodes to quasi-solid/liquid states (Prasianakis et al., 2018; Sukop & Thorne, 2006).

The discrete Lattice Boltzmann equations are particularly suitable for the parallel numerical algorithm due to the locality of the LB operator. In most practical implementations of the LB equations the communication and exchange of information is only required between the immediate neighbouring nodes. This allows for (a) simple implementation of complex boundary geometries, essential for simulating porous materials and (b) efficient parallelization of the algorithm for use in high performance computing facilities (Prasianakis et al., 2018). The algorithm parallel efficiency makes it ideal for use with massively parallel architectures such as graphics processing units (GPUs) as well as in hybrid CPU/GPU supercomputers (Kuznik, Obrecht, Rusaouen, & Roux, 2010; Safi, Prasianakis, & Turek, 2017). Their structural efficiency for parallel data allows to achieve speedups up to several orders of magnitude compared to an equivalent conventional CPU processor (Kuznik et al., 2010). Furthermore, the small amount of exchangeable data between computing nodes means that LB algorithm can be very efficient on interconnected GPU networks.

The LB model however, describes only the mass transport in fluid and the fluid-solid interface evolution. The chemical equilibria calculations need to be implemented and coupled via separate thermodynamic modelling routines. Geochemical speciation solvers provide the quantities of chemical speciation and phase stability in the system under the assumption of local equilibrium. These calculations can be done using the Law of Mass Action (LMA) (as in PhreeqC (Parkhurst, 1995)) or Gibbs Energy Minimization (GEM) (as in GEMS-Selektor (Kulik et al., 2013)). Due to the complexity of the calculations of thermodynamic equilibrium and geochemical speciation, the chemical model cannot match the efficiency of the LB algorithm on calculating the mass transport on a single computational grid point for a given time step. With chemistry being the bottleneck, coupling of the two aforementioned codes leads to an unbalanced code that spends the vast majority of its calculation time in the thermodynamic modelling routines (Y. Huang et al., 2018). This is due to the large number of involved species and the

EURAD Deliverable 16.8 – MAGIC - S/T 4-1 – 4/2 -Chemo-mechanical numerical coupling development and up-scaling methods

need to perform chemical calculations at each mesh point and every time step. In addition, chemical and mass transport time scales differ significantly.

To improve performance of geochemical calculation we replace native geochemical solvers (Laloy & Jacques, 2022; Prasianakis et al., 2020) with its surrogate models (Jain, Jianchang, & Mohiuddin, 1996) using highly accurate and numerically efficient artificial neural networks (ANN). The ANN are trained for the system of interest by a supervised learning approach using the data from the native geochemical solver (e.g. GEMS-Selektor (Kulik et al., 2013)). Extensive benchmarking exercises have demonstrated that the feedforward type of neural networks are one of the simplest but most efficient network types, suitable for solving complex regression problems (Laloy & Jacques, 2022; Prasianakis et al., 2020). The training is done using the backpropagation technique (Rumelhart, Hinton, & Williams, 1986). At the moment, it seems that for an arbitrary system different types and structures of ANN need to be tested, as the optimal configuration is not known a priori.

The LB reactive transport algorithm is implemented in two codes: (a) a CPU-based Python-Fortran code coupled with PhreeqC (Ravi A. Patel, Churakov, & Prasianakis, 2021; R. A. Patel et al., 2014) for small scale 2D/3D domains, with full coupling between the LB and the thermodynamics calculation and (b) a GPU-based CUDA/C++ code (Safi et al., 2017) coupled with a pre-trained (through GEMS-Selektor thermodynamics calculations) surrogate model. The latter code can be used for large-scale 3D domains described by more than 1 billion computational grid points, where performing chemical calculations via typical thermodynamic modelling routines becomes computationally unfeasible.

Simulations have been conducted with the GPU-based CUDA/C++ code (Safi et al., 2017) for the dissolution of CH in a 3D microstructure. The cubic domain of volume $100\mu\text{m}^3$ was produced by the HYMOSTRUC code (van Breugel, 1995) and discretised with particle spacing $1\mu\text{m}$. The microstructure was provided by SCK-CEN and it was based on Ordinary Portland Cement and is similar to (Ravi A. Patel et al., 2021; R. A. Patel et al., 2014; Varzina et al., 2020).

The portlandite dissolution was implemented in the LB code through an equation based on the transition state theory (Lasaga, 2014), which was implemented as a source term in the LB equation. The necessary physical constants for the reaction were identified from experimental results (Galan, Glasser, Baza, & Andrade, 2015; Johannsen & Rademacher, 1999). Figure 1.1-1 **Erreur ! Source du renvoi introuvable.** shows a comparison between the domain state at the beginning of the simulation and after 1.5 million LB steps or 2136.75s (1 LB time step = 0.0014245s). At this point, approximately 68.7% of the portlandite has been dissolved. Leaching was considered only if the portlandite was in contact with the liquid, signified by the red nodes in Figure 1.1-1. It should be mentioned that in this simulation the CSH phase is considered inert.

Additional simulations have been conducted to investigate the sensitivity of the dissolution to the mineral surface reactivity. This is aimed at the evaluation of the effect of microbial activity on the evolution of the cement microstructure. Microbial activity is expected to modify the porosity through increased precipitation of secondary mineral phases followed by an alteration and dissolution of cement minerals. Further details on the LB portlandite dissolution simulations, including a detailed description of the model and the effects of reactivity can be found on deliverable D16.7 for Task 3. The same report (D16.7) also contains the details of the investigation of the effect of the temporal and spatial evolution of both the chemical composition and the cement microstructure to the mechanical properties of cement and concrete as part of a synergistic collaboration (PSI, SCK-CEN, LAMCUBE). The results were upscaled to the concrete scale as required by Subtask 3.4.

Additional simulations are underway for the investigation of the effect of CSH leaching in the microstructure. The model being benchmarked against the experimental data on cement paste degradation carried out by PSI/Empa as part of Subtask 3.1, which investigate the mechanical, microscopic and mineralogical characterisation of newly casted OPC and ESDRED mortars (<https://igdtp.eu/activity/esdred-engineering-studies-and-demonstrations-of-repository-designs/>). The specimens were exposed to an Opalinus clay pore solution and have been compared to 9-year aged

mortars obtained from the Mont Terri experimental site (Mäder et al., 2018), examined as part of Subtask 2.2. The aim would be for the simulations to use the specimens' microstructure (if available) or a chemical or mechanical equivalent. The definition of an interface to transfer these properties to macroscopic thermo-hydro-mechanical codes are conducted within Subtask 4.1.

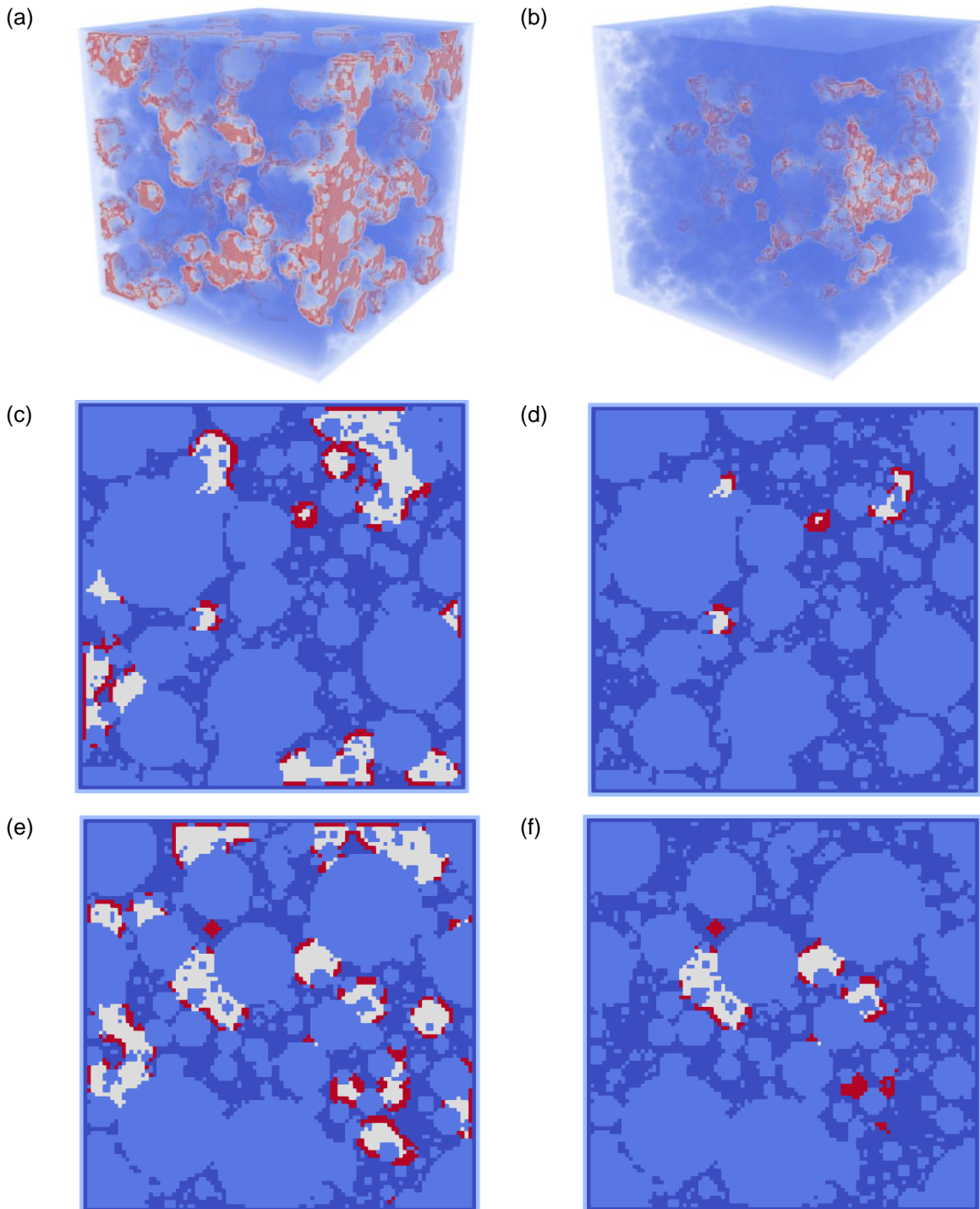


Figure 1.1-1: Ca leaching LB simulations, considering the dissolution of portlandite. The left column shows the initial state, while the right shows the state after 1.5 million LB steps. Red nodes signify correctly dissolving portlandite, white nodes are inactive portlandite not in contact with liquid, light blue signify inactive CSH and aggregates and dark blue is water. a) and b) show the full 3D microstructure, c) and d) show a 2D slice at 30 μm from the edge and e) and f) show a 2D slice at 60 μm from the edge

1.2 Chemo-mechanical models in saturated environment (led by LMDC)

The durability of underground structures for nuclear waste disposal is a critical aspect of nuclear waste management. These structures must be able to resist extreme environmental and mechanical conditions for long term (Figure 1.2-1). The presence of water in the underground disposal environment can cause various chemical reactions due to the ionic exchanges around the disposal facility. During certain stages of waste disposal operations, two main chemical reactions take place: the leaching of calcium coupled with the carbonation process. These reactions are influenced by temperature cycles that can reach up to 70°C during the disposal of nuclear waste. These temperature fluctuations will dry out the interior of the facility which evolve the relative humidity. In addition to these environmental aggressions, the tunnel is subjected to mechanical loading due to soil convergence. Therefore, the prediction of the behaviour of these structures over a thousand years requires a thermo-hydro-chemical and mechanical coupling model (Prasianakis et al., 2018; Sukop & Thorne, 2006).

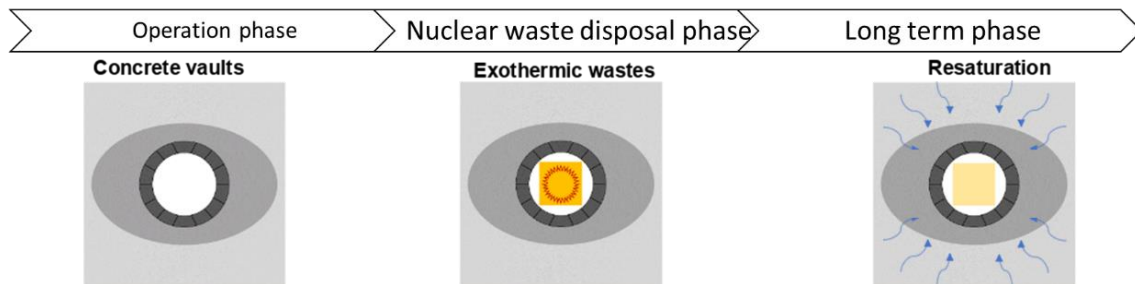


Figure 1.2-1: Service life of the disposal structure

The main objective of this work is to establish a finite element model able to consider the effects of site water and long-term mechanical loading on reinforced concrete structure. The global approach is divided for three parts (Figure 1.2-2):

1. A finite element model to predict the evolution of temperature, water saturation (of concrete and ground) and the chemical degradation of concrete (leaching and carbonation). This model will be based on the mineralogy of the cement paste.
2. Successive homogenization model for the paste in order to consider the case of reinforced concrete and to couple the chemical model with the mechanical model. This model will allow to reflect the effect of chemical degradation on the mechanical properties of reinforced concrete (Young modulus, creep...).
3. Apply the model in the scale of the structure (Base case) to predict the mechanical behaviour on long-term.

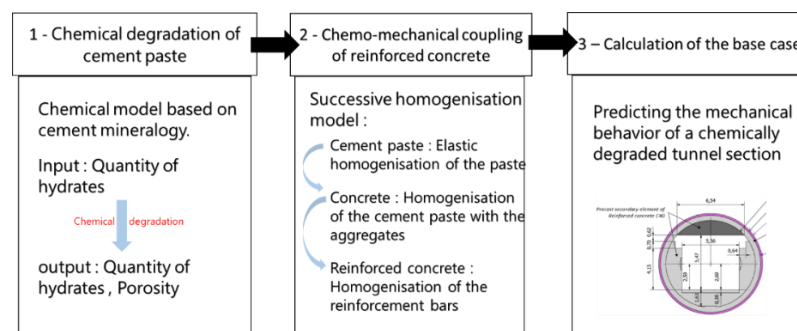


Figure 1.2-2: Global approach scheme

This report will focus on the model of the chemical degradation of the cement paste. For instance, the model couples the leaching of calcium and the carbonation of the cement paste at a constant degree of saturation. This model takes into account the effect of temperatures and the cement mineralogy.

1.2.1 Strategy for model reduction

The model must predict the different evolutions that occur during the lifetime of the structure. The modelling of these evolutions is described by the equations of mass conservation and energy. Furthermore, as the exact formulation of the concrete used in the disposal structures is not yet determined, the model must be adaptable to various formulations and consider the initial mineralogy of the material. The variables of the thermo-hydro-chemical model should characterize the different occurrences and the initial composition of the cement paste. The Table 1.2-1 represent all the variables \bar{X} of the THC model. The purpose of this work is to predict the mechanical behaviour of a structure. Therefore, the reduction of the size of the chemical model is necessary to couple it efficiently with the mechanical calculations. This reduction in the size of the chemical model aims to reduce the number of state variables to be managed based on the hypothesis of instantaneous dissolution. Thus, this model is reduced to four variables states \bar{Y} shown in the Table 1.2-1 able to describe the different phase of the disposal structures. Note that the other variables remain internal variables in the model.

Table 1.2-1 variables of the chemical degradation model of the cement paste

Variables of the THC Model	States Variables
X ₁ : Temperature	Y ₁ : Temperature T
X ₂ : Mass of liquid water X ₃ : Mass of vapour water	Y ₂ : Pressure of the liquid P _L
X ₄ : Carbon dioxide in aqueous form X ₅ : Carbon dioxide in gazes form	Y ₃ : Carbon dioxide in aqueous form CO _{2(aq)}
X ₆ : Calcium in porous media X ₇ : Portlandite X ₈ : Ettringite X ₉ : Mono sulphate X ₁₀ : Hydro garnet X ₁₁ : CSH _{(c/s)max} X ₁₂ : CSH _{(c/s)0,85}	Y ₄ : Calcium in porous media Ca ²⁺

The conservation of mass equation for all \bar{X} is written in a general form as follows:

$$1, \tag{1.2-1}$$

where: - C_i capacity of species Xi

- $D_i(\bar{X})$ coefficient of diffusion

- $S_{j \rightarrow i}(\bar{X})$ source involving in Xi

Then, the equivalent mass conservation equation is written in term of the variables states \bar{Y} as follows:

$$C_{eq} \frac{\partial Y_K}{\partial t} + \text{div} \left[-D_{eq}(\bar{X}, \phi, S_L) \cdot \overrightarrow{\text{grad}} Y_K \right] = S_{eq}(\bar{X}), \quad 1.2-2$$

Where: - C_{eq} equivalent capacity of species Y_K

- $D_{eq}(\bar{X})$ equivalent diffusion term

- $S_{eq}(\bar{X})$ equivalent source term involving in Y_K

1.2.1.1 Leaching of calcium

The modelling of calcium leaching at macro scale is based on the hypothesis that calcium in solution is in instantaneous equilibrium with solid calcium in the cement matrix as the calcium is the main element in the cement matrix. The evolution of the calcium in the solid matrix as a function of the calcium concentration in the pore solution is represented by the thermodynamic equilibrium curve.

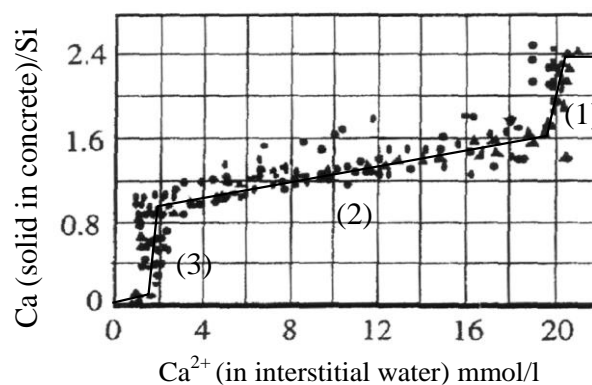


Figure 1.2-3 Thermodynamic equilibrium curve at 25°C (Gerard, Pijaudier-Cabot, & Laborderie, 1998)

This curve depends on temperature, it shifts to the left with temperature increasing and the range of calcium concentrations at equilibrium in the pore solution decreases.

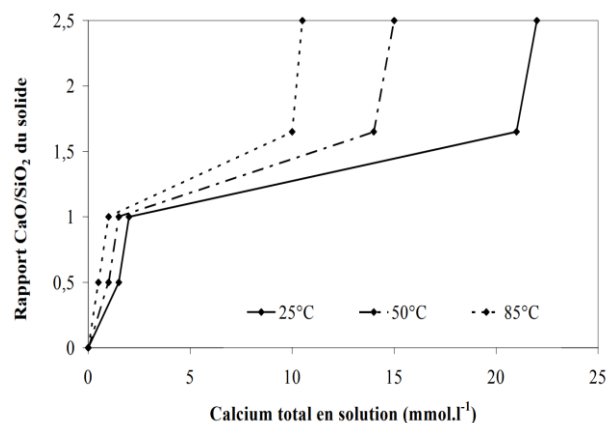


Figure 1.2-4 Effect of temperatures on the equilibrium curve (Peycelon, Blanc, & Mazoin, 2006).

In order to model this curve considering the effect of temperature and cement mineralogy, a function f has been proposed to describe the dissolution of each hydrate. This function varies between 0 and 1, and depends on the equilibrium concentration of calcium at temperature T , m and $k(m)$ are parameters to be adjusted for each hydrate. Thus, the evolution of calcium in solid phases as a function of calcium

in solution is obtained by multiplying by the maximum amount of calcium in each hydrate (Equation 1.2-4). The resulting equilibrium curve is the sum of the elementary curves of all hydrates.

$$f_{Xi}(Ca^{2+}) = 1 - \exp \left[\frac{-1}{m} \left(\frac{[Ca^{2+}]}{k^{(m)}[Ca_{eq}^{2+}(T)]} \right)^m \right] \quad 1.2-3$$

$$Cas_{Xi}(Ca^{2+}) = f_{Xi}(Ca^{2+}) \times Cas_{max_{Xi}} \quad 1.2-4$$

The effect of temperature on the equilibrium concentration of calcium can be expressed as follow:

$$[Ca_{eq}^{2+}(T)] = [Ca_{eq}^{2+}(T_0)] \exp \left[-\frac{E_A}{R} \left(\frac{1}{T} - \frac{1}{T_0} \right) \right] \quad 1.2-5$$

E_A is a constant allowing to fit the dependence of equilibrium concentration in calcium on temperature for each hydrate and R is the ideal gas constant.

1.2.1.2 Elementary curve of portlandite

The equilibrium concentration of calcium for the dissolution of portlandite is obtained by a thermodynamic calculus using the least square method

$$[Ca^{2+}][OH^-]^2 = 10^{-pK(25^\circ C)} \rightarrow [Ca_{eq}^{2+}(25^\circ C)]_{CH} = 22 \text{ mmol/L} \quad 1.2-6$$

The elementary equilibrium curve for the portlandite is represented in the figure. The shape of this curve avoids the sudden dissolution of the hydrate and make the dissolution smoother, which allow the model to converge in a reasonable time.

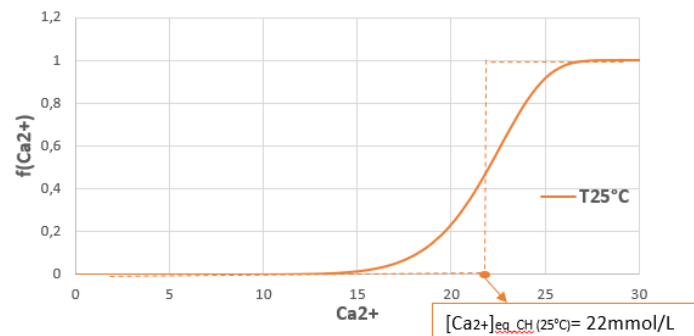


Figure 1.2-5 : Elementary equilibrium curve for the portlandite

Using the dependance on temperature of calcium at equilibrium, as mentioned in the Equation 1.2-5, the effect of temperature of the curve is represented in the bellow figure.

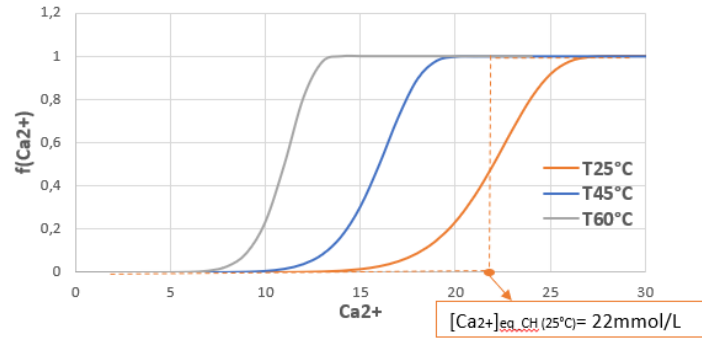


Figure 1.2-6 Effect of temperature on the equilibrium curve of the portlandite.

1.2.1.3 Equivalent mass conservation equation of calcium in solution

The mass conservation equation for calcium in solution is written in the Equation 1-7.

$$C_6 \frac{\partial X_6}{\partial t} + \text{div} \left[-D_6(\bar{X}, \phi, S_L) \cdot \overrightarrow{\text{grad}} X_6 \right] = \sum_{j=7}^{12} S_{6 \rightarrow j}(\bar{X}) + S_{CaCO_3} - X_6 \frac{\partial C_6}{\partial t} \quad 1.2-7$$

The term $\sum_{j=7}^{12} S_{6 \rightarrow j}(\bar{X})$ represents the calcium source term with describes the dissolution of all hydrates according to the equilibrium curve described above (equation **Erreur ! Source du renvoi introuvable.**).

This term is obtained by the derivate of the equation **Erreur ! Source du renvoi introuvable.**

$$\sum_{j=7}^{12} S_{6 \rightarrow j}(\bar{X}) = - \sum_{i=7}^{12} \frac{\partial C a s_i(Y_4)}{\partial Y_4} \frac{\partial Y_4}{\partial t} \quad 1.2-8$$

S_{CaCO_3} this term is due to the precipitation of calcite and the coupling with the carbonation (Equation 1.2-9). τ is a parameter which represents the time characteristic.

$$S_{CaCO_3}(\bar{Y}) = - \frac{Y_4 \cdot Y_3}{\tau} \quad 1.2-9$$

Thus, the equivalent mass conservation equation of calcium is written

$$\left[C_6 + \sum_{i=7}^{12} \frac{\partial C a s_i(Y_4)}{\partial Y_4} \right] \frac{\partial Y_4}{\partial t} + \text{div} \left[-D(\bar{X}, \phi, S_L)_6 \cdot \overrightarrow{\text{grad}} Y_4 \right] = - \frac{Y_4 \cdot Y_3}{\tau} - Y_4 \frac{\partial C_6}{\partial t} \quad 1.2-10$$

1.2.1.4 Diffusion coefficient of calcium

The coefficient of diffusion should consider the effect of saturation and porosity. The cement paste diffusion coefficient adapted for CEMI is described in the equation 1.2-11 (Tognazzi-Lawrence, 1998) (Bary & Sellier, 2004)

$$K(sl) = \frac{1}{(1 + 625(1 - sl)^4)} \quad 1.2-11$$

$$De(Ca) = 2,3 \cdot 10^{-13} \exp(9,95\phi)$$

$$D_{Ca} = K(sl) \cdot De(Ca)$$

The effect of temperature is expressed by the Arrhenius law in equation 1.2-10. E_A is the energy activation corresponding to the diffusion of calcium.

$$D_{Ca} = D_{Ca0} \exp \left[-\frac{E_A}{R} \left(\frac{1}{T} - \frac{1}{T_0} \right) \right] \quad 1.2-12$$

1.2.1.5 Carbonation process

The carbonation of concrete is a process where the carbon dioxide dissolves and penetrate into the concrete containing Ca in solid phase to form the calcium carbonate. The modelling of the carbonation at macro scale is based on the mass conservation equation for the carbon dioxide in gaseous form and liquid form dissolved in the pores of the concrete. The dissolution of carbon dioxide gas into liquid is expressed by Henry's law and the perfect gas law:

$$[CO_2]_g = \frac{[CO_2]_{aq}}{R \cdot T \cdot H_{CO_2}(T)} \quad 1.2-13$$

$$[CO_2]_g = K_H(T) \cdot [CO_2]_{aq} \rightarrow X_5 = K_H(T) \cdot Y_3$$

The mass conservation equation for carbon dioxide in aqueous form:

$$C_4 \frac{\partial X_4}{\partial t} + \text{div} \left[-D_4(\bar{X}, \phi, S_L) \cdot \overrightarrow{\text{grad}} X_4 \right] = S_{5 \rightarrow 4}(\bar{X}) + S_{CaCO_3} - X_4 \frac{\partial C_4}{\partial t} \quad 1.2-14$$

The mass conservation equation for carbon dioxide in gaseous form:

$$C_5 \frac{\partial X_5}{\partial t} + \text{div} \left[-D_5(\bar{X}, \phi, S_L) \cdot \overrightarrow{\text{grad}} X_5 \right] = S_{4 \rightarrow 5}(\bar{X}) - X_5 \frac{\partial C_5}{\partial t} \quad 1.2-15$$

According to the assumption of the instantaneous dissolution between the two phases of carbon dioxide:

$$S_{5 \rightarrow 4}(\bar{X}) = -S_{4 \rightarrow 5}(\bar{X}) \quad 1.2-16$$

Combining the two-conservation equation 1.2-14 and 1.2-15. The equivalent mass conservation for carbon dioxide is:

$$\begin{aligned} [C_4 + K_H C_5] \frac{\partial Y_3}{\partial t} + \text{div} \left[-(D(\bar{X}, \phi, S_L)_4 + K_H(T) \cdot D(\bar{X}, \phi, S_L)_5) \cdot \overrightarrow{\text{grad}} Y_3 \right] \\ = S_{CaCO_3}(Y) - Y_3 \left(\frac{\partial C_4}{\partial t} + K_H(T) \cdot \frac{\partial C_5}{\partial t} \right) \end{aligned} \quad 1.2-17$$

1.2.1.6 Coefficient of diffusion of carbon dioxide

The apparent diffusion coefficient for carbon dioxide is formulated to consider the effect of saturation and the porosity of the cement paste (Ishida & Maekawa, 2000) (Ishida & Maekawa, 2000) (Thiery, 2005). The temperature dependency of the diffusion coefficient is expressed by Arrhenius law (Equation 1.2-19). $D_{CO_2}^0$ is the diffusivity of carbon dioxide in free atmosphere and $D_{CO_2}^0$ the diffusivity of dissolved carbon dioxide in pore water.

$$D_{CO_2^g} = D_{CO_2^g}^0 \cdot \phi^{2.74} \cdot (1 - S)^{4.2} \cdot f(T) \tag{1.2-18}$$

$$D_{CO_2^l} = D_{CO_2^l}^0 \cdot \frac{\phi \cdot S^4}{\Omega} \cdot f(T) \quad ; \quad \Omega = \left(\frac{\pi}{2}\right)^2$$

$$f(T) = \exp\left[-\frac{E_A}{R}\left(\frac{1}{T} - \frac{1}{T_0}\right)\right] \tag{1.2-19}$$

1.2.2 Model implementation

The mass conservation equations are implemented in the finite element code Cast3M. The use of geochemical software based on equilibrium, kinetic and reactive transport calculations, which are highly non-linear, is not compatible with the reasonable calculation time for a structure. Hence, the finite element code Cast3m, which is well suited to the mechanical calculation of structures, was chosen to implement the THMC model. The implicit method is used to solve the problem. The principle of solving these equations is based on iterative procedures (Figure 1.2-7).

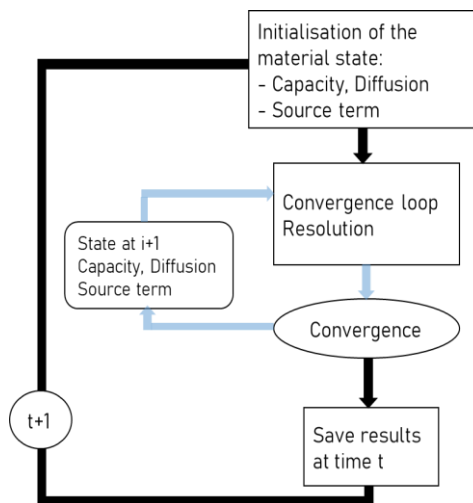


Figure 1.2-7 Algorithm of resolution.

At the beginning of the time step, the capacity and diffusion term of the material are initialized and also the source term of the conservation equation. Once the initial state is identified, the resolution of the equations starts in the convergence loop where at each iteration the capacity, diffusion and source terms are updated until the convergence criterion is verified.

The validation of the model and the tuning of the parameters are in progress and will be reported in D16-9 (end of December 2023). The validation will be divided into two parts, the validation of the calcium leaching model for different temperatures only and the validation of the carbon dioxide process for different carbon dioxide concentrations and at different temperatures on its own (Bary & Sellier, 2004).

1.3 Fracture formation and propagation models (led by UFZ)

We present a fully coupled chemo-hydro-mechanical (CHM) variational phase field model for simulating fracture initiation and propagation including chemical reactions in cementitious systems. The numerical model is implemented in the OpenGeoSys research software platform (www.opengeosys.org).

1.3.1 Coupled processes

We coupled three subprocesses: (i) reactive transport, (ii) fluid flow in porous media, and (iii) mechanical deformation of fractured porous media using variational phase-field in a staggered approach (Figure 1.3-1).

Reactive transport. We use the geochemical package PHREEQC coupled in an operator-splitting approach with a finite element transport solver to calculate chemical reactions in thermodynamic equilibrium (dissolution or precipitation) while taking into account changes in porosity (Lu et al., 2022).

Mechanical deformation of fractured porous media using variational phase-field. The linear poroelasticity theory proposed by Biot (Biot, 1941) has been used to model porous media deformation. As we consider fracture propagation in cementitious systems, we use the variational phase field approach to compute fracture nucleation and propagation without re-meshing and path identification in fractured porous media (Bourdin, Francfort, & Marigo, 2008).

Fluid flow in porous media. A local continuity equation can describe fluid flow in a saturated porous media based on mass conservation. Fluid transport was also computed based on the Darcy's law, an empirical equation for seepage flow in porous media that is non-deformable. We couple mechanical deformation and fluid flow using the fixed-stress splitting approach.

The proposed model was implemented in the open-source finite element framework OpenGeoSys (Bilke et al., 2019).

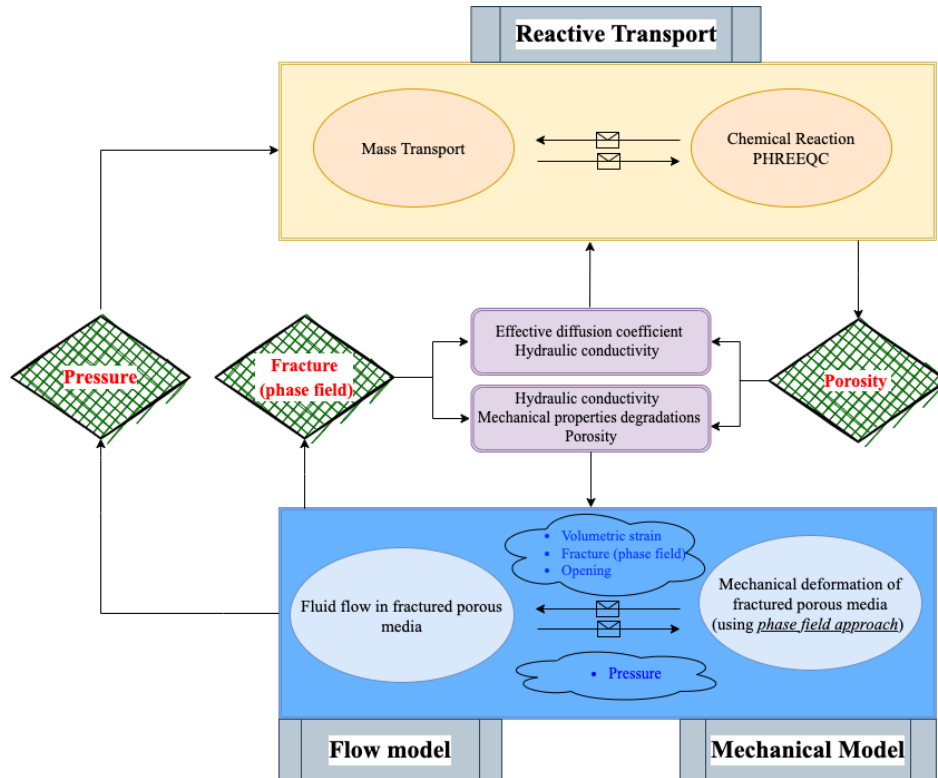


Figure 1.3-1 Fully coupled chemo-hydro-mechanical variational phase field model.

Griffith criterion (Griffith, 1921) reads a follow:

$$-dW(\mathbf{u})/dl \leq G_c \tag{1.3-1}$$

where $W(\mathbf{u})$ and G_c are the strain energy density and the fracture toughness, respectively. Griffiths' theory is straightforward but has limitations such as the assumption of a known propagation path and the inability to manage fracture nucleation. Francfort and Marigo (Francfort & Marigo, 1998) recast Griffith's theory as the minimization of total energy, which is the sum of strain and fracture surface energy:

$$\mathcal{F}(\mathbf{u}, \Gamma) = W(\mathbf{u}) + G_c H^{N-1}(\Gamma), \tag{1.3-2}$$

where G_c is the material's critical surface energy release rate and $H^{N-1}(\Gamma)$, denotes the $N - 1$ dimensional Hausdorff measure of Γ (crack set), which is an aggregate crack surfaces in three dimensions and an aggregate crack length in two dimensions. In a discrete time setting, identifying the displacement reduces to minimizing \mathcal{F} with respect to any kinematically admissible displacement \mathbf{u} and crack set Γ satisfying a growth constraint.

In terms of crack geometry, it is challenging to numerically represent the crack surface energy because the surface integral extends over an evolving discrete crack set Γ . In order to solve this issue, Bourdin et al. (Bourdin et al., 2008) proposed a variational phase field model that consists of a scalar phase field variable, $v: \Omega \mapsto [0,1]$, and a regularization length parameter, $\ell > 0$. In regularized form, the total energy is as follows (Bourdin et al., 2008)

$$\mathcal{F}_\ell = \int_\Omega v^2 W(\mathbf{u}) \, d\Omega + \int_\Omega \frac{G_c}{2} \left(\frac{(1-v)^2}{\ell} + \ell |\nabla v|^2 \right) \, d\Omega \tag{1.3-3}$$

1.3.2 The influence of the phase field and changes in porosity on the coupling process

Effective diffusion, hydraulic conductivity, and mechanical constitutive relations would be impacted by fracture and changes in porosity brought on by chemical processes.

1.3.2.1 Coupling diffusion coefficient, porosity, and phase field

As effective diffusion increase in the presence of fracture and changes in porosity, phase field variable and chemical damage should impact the diffusion coefficient (Wu & Chen, 2022) (Schuler, Ilgen, & Newell, 2020)

As the porosity increases, we will have (Schuler et al., 2020)

$$D(\phi_e) = D_p + D_0\phi_e^2 \quad 1.3-4$$

where D_p and D_0 denote pore diffusion coefficient and molecular diffusion, respectively; ϕ_e is effective porosity and which can be defined as:

$$\phi_e = \begin{cases} 0 & \text{for } \varphi_T \leq \varphi_c \\ a(\phi_T - \phi_c)^\beta & \text{for } \varphi_T \geq \varphi_c \end{cases} \quad 1.3-5$$

where $a = 2.4$ and $\beta = 0.9$ are model parameters; φ_c and φ_T are critical and total porosity.

The following equation describes how mechanical damage (phase field) may affect the diffusion coefficient (Gerard et al., 1998)

$$D(v) = D_p + D_0 \left(1 - \frac{1}{1 + \left(\frac{1-v}{d_{cr}} \right)^n} \right), \quad 1.3-6$$

where $d_{cr} = 0.4$ and $n = 5$.

The diffusion coefficient is chosen to reflect the greatest variation between chemical and mechanical diffusions (Schuler et al., 2020)

$$D(\phi_e, v) = \max(D(\phi_e), D(v)) \quad 1.3-7$$

1.3.2.2 Influence of chemical dissolution in constitutive relationships

For chemical damage, we introduce a variable to a constitutive relation that represents a degree of chemical damage ranging from zero (intact) to one (damaged material). The chemical damage variable represents changes in porosity caused by chemical reactions independently from the phase field variable that represents the mechanical damage (Gerard et al., 1998). Gerard et al. (Gerard et al., 1998) revised the stress-strain relationship as follows, including chemical damage, $V(\varphi)$:

$$\sigma_{ij} = g(v)(1 - V(\varphi))C_{ijkl}\varepsilon_{kl} \quad 1.3-8$$

$V(\varphi)$ is a function of porosity and can be defined in different ways (Wu & Chen, 2022):

$$V(\varphi) = \begin{cases} \Delta\varphi & \text{for leaching} \\ 1 - \exp(-\gamma\Delta\varphi) & \text{for dissolution in rock} \end{cases} \quad 1.3-9$$

where $\gamma=10$ is an empirical coefficient.

1.3.2.3 Coupling Permeability, porosity changes, and phase field

Additionally, in presence of fracture, the permeability, K , in Darcy law is decomposed as follow:

$$K = K_m + (1 - \nu)K_f, \quad 1.3-10$$

where $K_m = K/\mu l$ is the matrix hydraulic conductivity and K_f is permeability depend on fracture aperture. Also, the permeability will change with a change in porosity through empirical equations (e.g. Kozeny–Carman).

1.3.3 Preliminary results

The proposed model is implemented in the OpenGeoSys (OGS) package. Before we verify and validate the results, we have designed a benchmark to demonstrate the functionality of our implemented coupled system. This benchmark involves subjecting a saturated edge-fractured sample with a sand-calcite mixture to a tensile load, followed by injecting a 0.005M sulfuric acid solution targeting the sand-calcite mixture layer (see Figure 1.3-2). The primary goal of this benchmark is to illustrate how the presence of fractures and changes in porosity impact reactive transport.

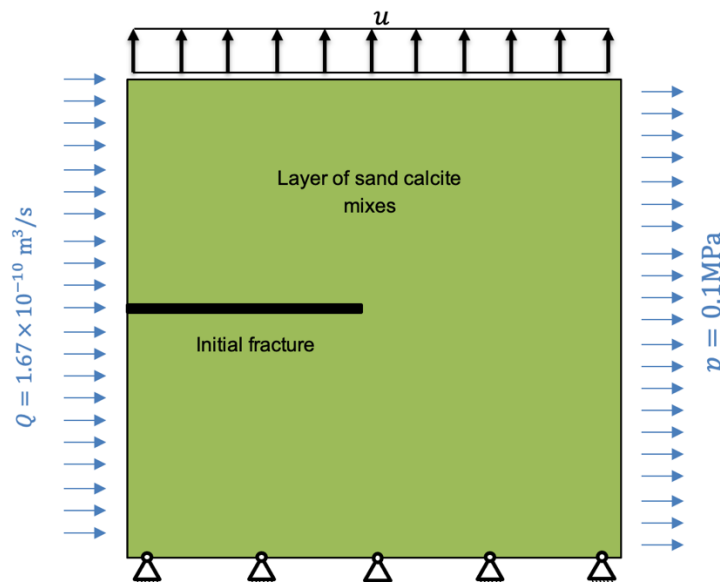
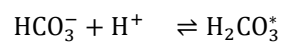
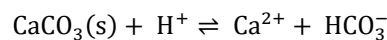


Figure 1.3-2 Schematic view a fully couple benchmark.

In terms of calcite dissolution reactions, we consider the following reactions:



To ensure the correctness of our implementation, we have established a series of benchmarks to assess the coupling between different processes:

- Hydro-Mechanical coupling (consolidation benchmark)
- Hydro-Phase Field (fluid flow in fracture benchmark)
- Hydro-Mechanical-Phase Field (KGD benchmark)
- Reactive transport
- Evaluating the impact of changes in porosity on mechanical deformation (degradation)
- Investigating the effect of changes in effective diffusion in the presence of fractures and changes in porosity

Once the verification process is finished, we will proceed with a real case study.

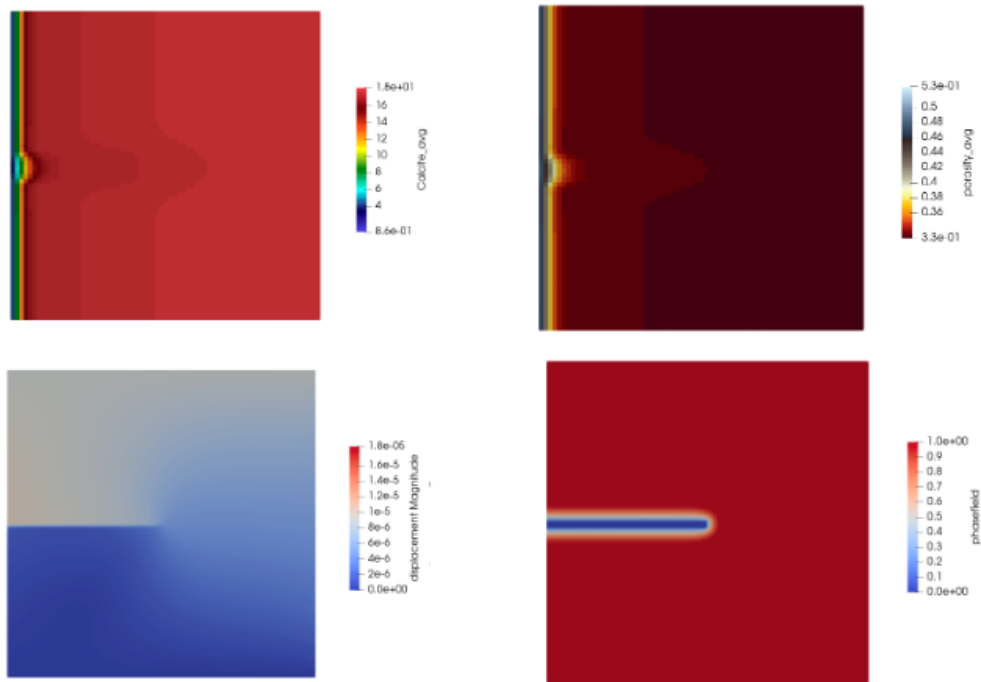


Figure 1.3-3 Profiles of calcite (top left), porosity (top right), displacement (bottom left), and phase field (bottom right) before fracture propagation.

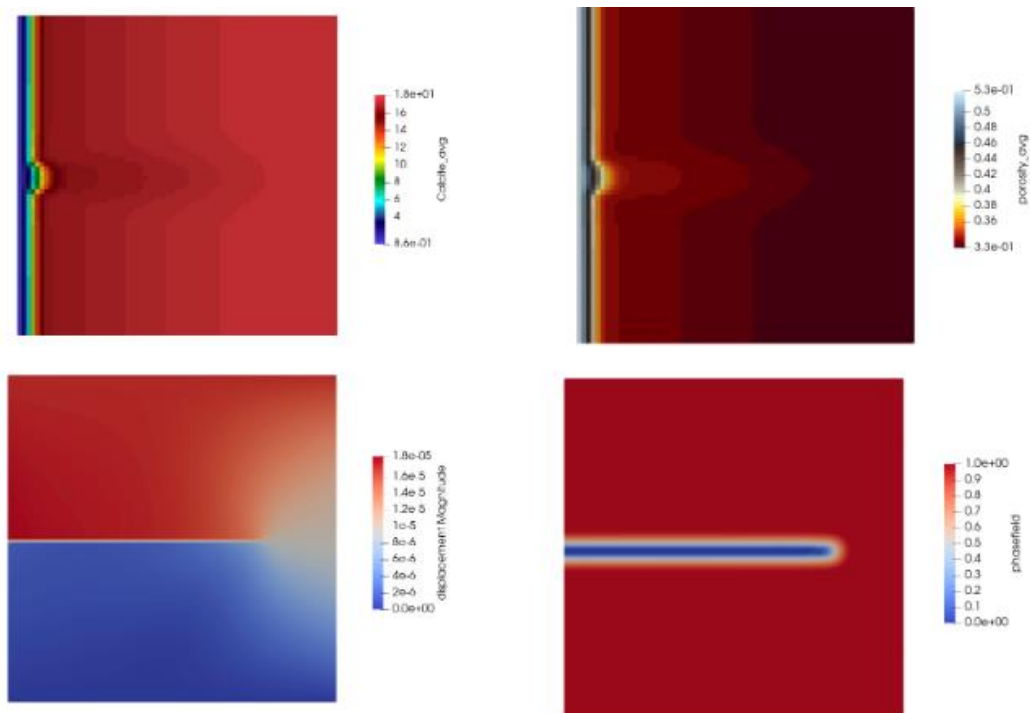


Figure 1.3-4 Profiles of calcite (top left), porosity (top right), displacement (bottom left), and phase field (bottom right) after fracture propagation.

1.4 Damage model in unsaturated conditions (led by CEA/Mines PSL)

1.4.1 Context and approach description

Carbonation is a complex degradation process which involves severe feedback mechanisms between hydraulic, chemical, mechanical and thermal effect. In a prior MAGIC publication (Nicolas Seigneur, De Windt, Poyet, Socié, & Dauzères, 2022), it was demonstrated that reactive transport alone was not able to represent the long-term effect of carbonation without incorporating the appearance and propagation of cracks. This implies that a fully coupled Thermal-Hydraulic-Mechanical-Chemical (THMC) approach is required to accurately model carbonation.

A literature review of past attempts to THMC approaches revealed that much remained to be done in this topic. In general, past attempts usually included two shortcomings:

- They never included a two-way dynamic feedback between chemistry and mechanics.
- The THMC (or reactive transport part) is usually simplified as it does not take into account the water production and consumption.

For concrete in general, water reactivity plays an important part for the durability of concrete and cementitious materials, as we have shown in (Nicolas Seigneur et al., 2022), for carbonation. Also, the induced pore-pressure is important to consider for a chemo-mechanical coupling, as emphasized by the drying shrinkage observed in these materials. Hytec capacities with respect to water reactivity were able to solve the second shortcoming (Nicolas Seigneur, Lagneau, Corvisier, & Dauzères, 2018). From this, a poromechanical calculation can be implemented with CAST3M, thanks to the Hytec computation of pore pressure and mineralogical fields. We have chosen a damage approach in CAST3M which can be converted into crack openings which would then be fed back in HYTEC through the double-porosity approach available in Hytec (Figure 1.4-1).

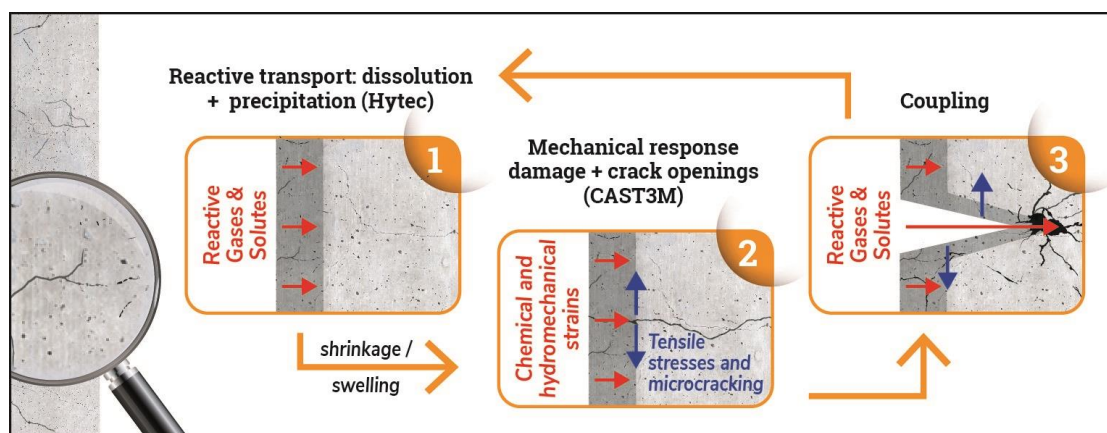


Figure 1.4-1: Illustration of the approach

Our approach has yielded very satisfying results for the model C_3S paste. Our approach is general and generic and can constitute a **gamechanger** for numerous THMC applications. For its disruptive nature, we have chosen to submit this to a Nature Portfolio Journal (Materials Degradation). Here below is a summary of the methodology and results, while more details are available in the associated publication

1.4.2 Methodology

1.4.2.1 Reactive transport

The reactive transport approach is the same as the one given in (Nicolas Seigneur et al., 2022) but includes a dual-medium approach. The two media are the matrix (representing concrete, with a superscript m) and the cracks (superscript c). The interaction between these two domains depends on

the crack-network geometry. We represent it with its surface area A (m^2/m^3) and the crack characteristic length D .

In Hytec, we solve the Richards equation to compute the unsaturated flow problem in a dual-porosity media, with cross-continuum fluxes calculated based on a morphological parameter, associated to the crack aperture and lengths, which are computed from the poromechanical simulation. Average of permeability and relative permeabilities are used to calculate the Darcy-velocity between the two domains. All the equations are given in (Socié, Seigneur, Bary, Poyet, & Touzé, 2023).

Similarly, the reactive transport problem is written, for every component including water. The chemical solver computes the solid-liquid-gas equilibrium, the evolution of water content, solution density and porosity. The method is described in details in (Nicolas Seigneur et al., 2018) and in other applications papers (Nicolas Seigneur, De Windt, Déjeant, Lagneau, & Descostes, 2021; Nicolas Seigneur et al., 2022; N Seigneur et al., 2020). At the end of the RT timestep, the source terms in Richards equation are computed. The crack diffusive properties are computed using a Millington-Quirk relation and include a dependence on the crack aperture, governed by CAST3M.

The geochemical description which is used in our submission is the same than the one given in (Nicolas Seigneur et al., 2022).

1.4.2.2 Poromechanical damage approach

The poromechanical model includes material deformation and damage induced by the evolution of porosity, mineralogical and pore-pressure fields through a constitutive law. The latter includes the chemical shrinkage, as computed based on Hytec results, and the effect of pore-pressure. Poromechanical properties (Young's modulus, Biot coefficient) are evaluated based on a homogenization approach (Mori-Tanaka). The model can account for the mechanical response associated to a change in pore pressure, for example due to drying or gas pressure build-up through the Biot term. We have chosen a damage description through a classical damage scalar variable D , varying between 0 for sound material and 1 for totally degraded one. The crack opening displacement vector, noted $[u]$, calculated from the continuum damage model is based on Mathallah et al. approach (Matallah, La Borderie, & Maurel, 2010), which has been applied and validated in several studies involving concrete (Jourdain, 2014; Nilenius, Larsson, Lundgren, & Runesson, 2015; Sellier & Multon, 2018). Details on the approach and parameters are given in (Socié et al., 2023).

1.4.3 Results

Numerical results are presented and confronted to experimental observations in details in the published article (Socié et al., 2023) and an extraction of these results are presented in figures below. The carbonation depths and microcracks patterns are consistent with experimental observations. The latter can only be explained by the coupled chemo mechanical impacts which drive the appearance of cracks predominantly along the sample edges.

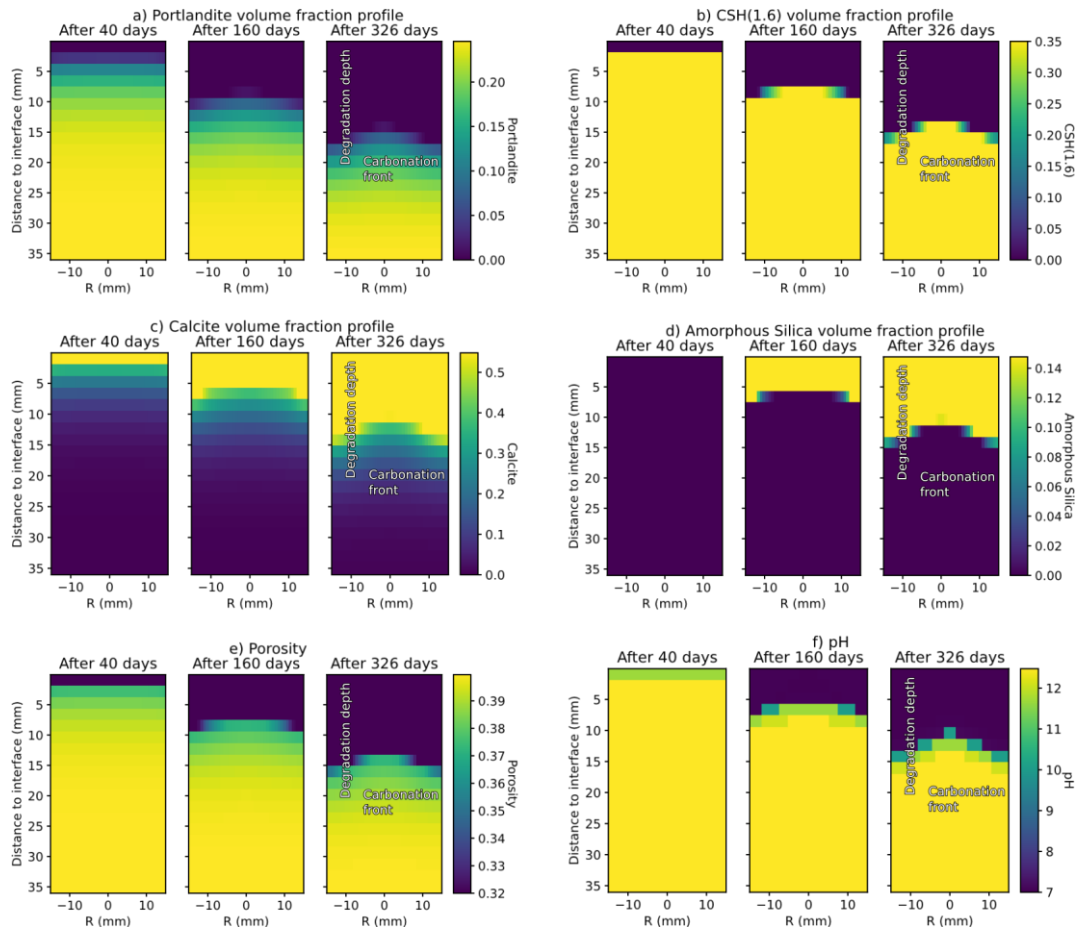


Figure 1.4-2 Mineralogical spatial maps after 40, 160 and 326 days of accelerated carbonation of the C₃S paste.

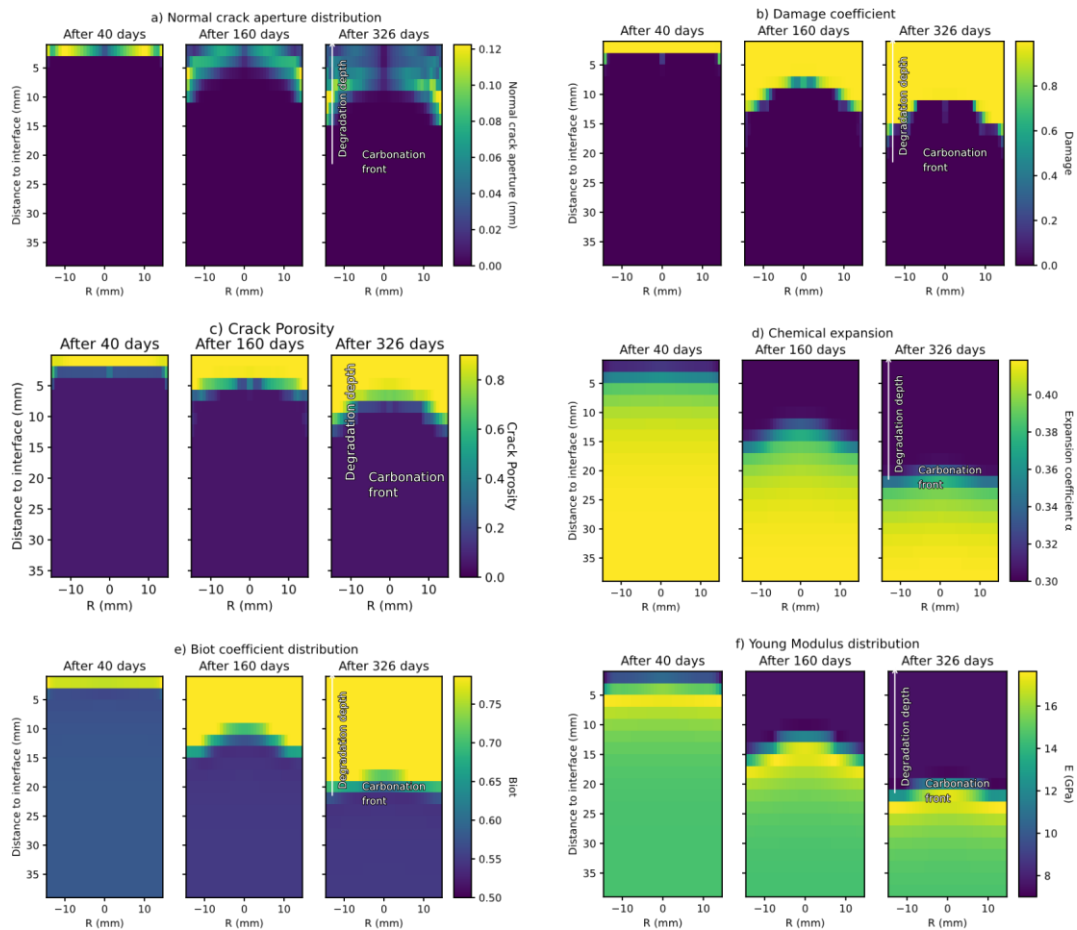


Figure 1.4-3 Mechanical spatial maps after 40, 160 and 326 days of accelerated carbonation of the C₃S paste.

1.4.4 Perspectives

The presented approach has overcome the main two shortcomings of THMC modelling and may be readily available for many contexts. For the investigated material, our approach is predictive: it is only parametrized by measured parameters (initial porosity, mineralogy, sorption isotherm, gas effective diffusion coefficient, thermodynamic data). We have not used any empirical factors and have chosen reasonable values and laws for every other parameters (homogenization laws for micromechanical properties, Millington-Quirk, ...). Hence, we believe that its extrapolation to other conditions can be successful, as long as the operational conditions are not dramatically different. For example, in case of extreme drying conditions, the impact of Millington-Quirk parameters will heavily influence the CO₂ migration. Our simulation has not been validated under such conditions.

Additional work could provide a deeper analysis of the influence of these parameters and laws. Additionally, the applications to another model material (a C-S-H paste) need to be improved.

2. Upscaling of mechanical properties vs cement alteration

2.1 Analytical homogenization (led by LAMCUBE)

2.1.1 Simplified micro-structure considered

The estimation of macroscopic mechanical properties is inherently based on the description of microstructures and the local mechanical properties of constituent phases. It is worth noticing that the microstructures of concrete materials are typically complex. For example, different types of Calcium Silicate Hydrate (C-S-H) are formed in cement paste. Voids and inclusions of different sizes are distributed at various scales. The macroscopic mechanical properties of concrete materials are fundamentally influenced by the local characteristics of constituent phases, their morphology, porosity, and the volumetric fraction of inclusions. Considering all these micro-structural parameters simultaneously poses challenges.

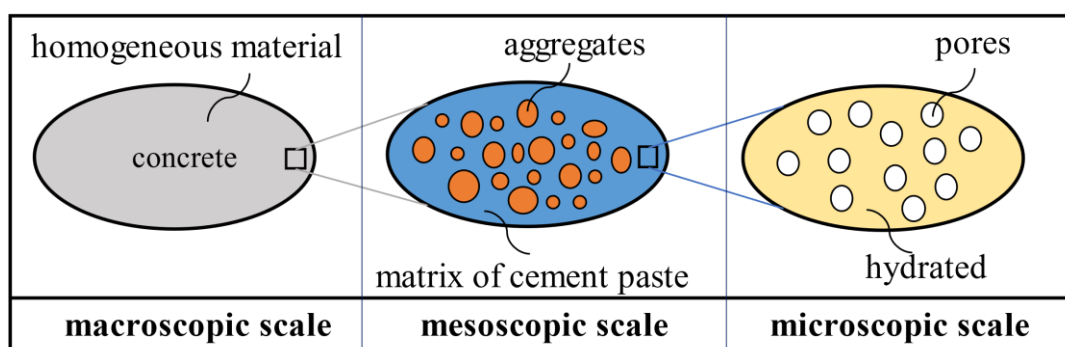


Figure 2.1-1 REV of concretes with pores and aggregates.

Building upon the methods introduced above, we consider here concrete materials containing a class of pores and a family of inclusions, each situated at different scales. The representative elementary volume (REV) of the concrete material is illustrated in Figure 2.1-1. At the macroscopic scale (cm), the material is represented as a homogenized equivalent medium (HEM), the strength properties of which need to be predicted. At the mesoscopic scale (Matallah et al.), aggregates are distributed in a quasi-continuous cement paste matrix. At the microscopic scale (μm), the cement paste contains a family of pores.

2.1.2 Chemical mechanical coupling

For the description of chemical mechanical coupling with the micro-mechanics-based modelling, the effects of chemical degradation are directly described by the evolution of microstructures. More precisely, due to chemical leaching, a part of solid calcium is dissolved and the related volume is transformed into an increase of porosity. As the mechanical properties are explicitly functions of porosity, its increase will directly affect the elastic properties and failure strength. Inversely, due to carbonation, there is a decrease of porosity and production of additional solid calcite grains. The elastic modulus and failure strength are then increased.

We are waiting for the experimental data from Task 2 and Task 3 to quantify the chemical degradation effects on micro-structural evolution and mechanical properties changes.

2.1.3 Elastic properties

Through two stages of homogenization, we derive analytical models for estimating the macroscopic elastic properties of concrete materials, as shown in Equations 2.1-1 and 2.1-2.

$$\kappa^{hom} = \frac{\frac{(1-\rho)\kappa^{pm}}{3\kappa^{pm} + 4\mu^{pm}} + \frac{\rho\kappa_i}{3\kappa_i + 4\mu^{pm}}}{\frac{(1-\rho)}{3\kappa^{pm} + 4\mu^{pm}} + \frac{\rho}{3\kappa_i + 4\mu^{pm}}} \quad 2.1-1$$

$$\mu^{hom} = \frac{\frac{(1-\rho)\mu^{pm}}{\mu^{pm}(9\kappa^{pm} + 8\mu^{pm}) + 6\mu_s(\kappa^{pm} + 2\mu^{pm})} + \frac{\rho\mu_i}{\mu^{pm}(9\kappa^{pm} + 8\mu^{pm}) + 6\mu_i(\kappa^{pm} + 2\mu^{pm})}}{\frac{(1-\rho)}{\mu^{pm}(9\kappa^{pm} + 8\mu^{pm}) + 6\mu^{pm}(\kappa^{pm} + 2\mu^{pm})} + \frac{\rho}{\mu^{pm}(9\kappa^{pm} + 8\mu^{pm}) + 6\mu_i(\kappa^{pm} + 2\mu^{pm})}} \quad 2.1-2$$

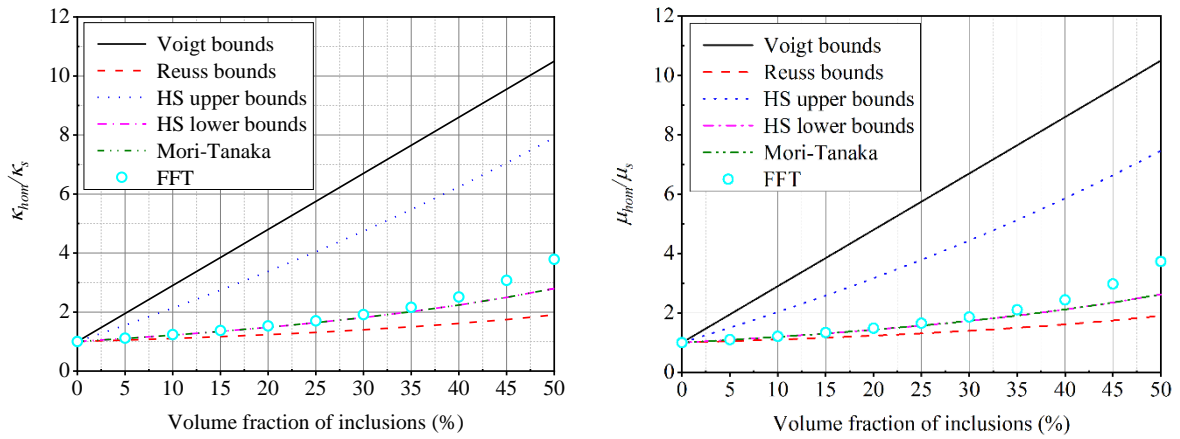
with the following coefficients:

$$\kappa^{pm} = \frac{4(1-\phi)\kappa_s\mu_s}{4\mu_s + 3\phi\kappa_s} \quad 2.1-3$$

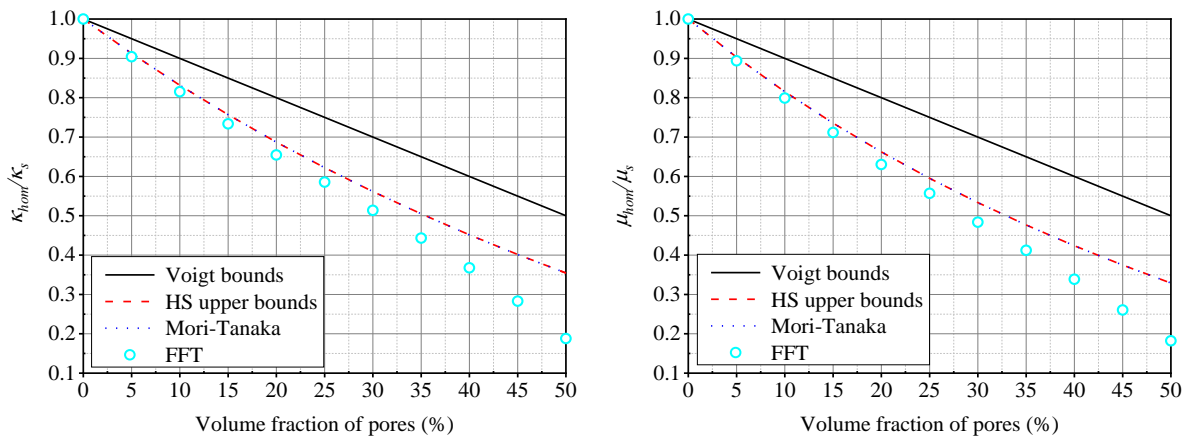
$$\mu^{pm} = \frac{(1-\phi)\mu_s}{1 + 6\phi \frac{\kappa_s + 2\mu_s}{9\kappa_s + 8\mu_s}} \quad 2.1-4$$

Where κ_s and μ_s are the bulk and shear moduli of the solid phase, κ_i and μ_i are the bulk and shear moduli of the inclusion. ρ represents the volume fraction of inclusions, ϕ is the porosity at the microscopic scale.

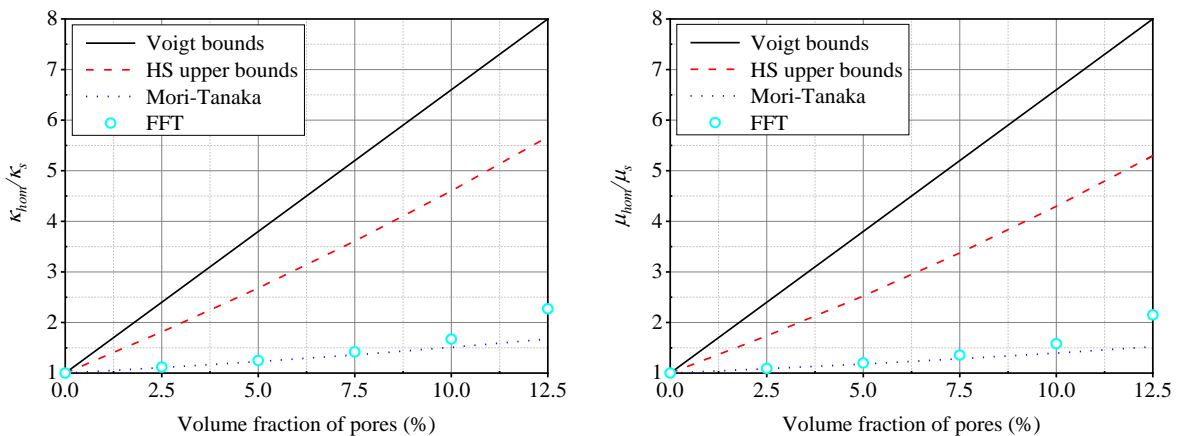
Furthermore, when investigating the elastic properties of concrete, it is essential to consider another prevalent microstructural configuration, which involves the coexistence of pores and inclusions at the same scale. Among the numerous analytical homogenization models used for estimating the macroscopic elastic properties of such composite materials, common fundamental models include the Voigt and Reuss bounds, Hashin-Shtrikman (HS) bounds, and the Mori-Tanaka (MT) estimation scheme. Firstly, we conducted a comprehensive evaluation of these four analytical models. In Figure 2.1-2, one shows the evolution of normalized macroscopic elastic moduli of materials with only inclusion (see Figure 2.1-2 (a)), only pores (see Figure 2.1-2 (b)) and both pores and inclusions (a representative case with an inclusion-pore ratio of 3:1 is selected, see Figure 2.1-2 (c)) respectively. The comparisons between the reference FFT solutions and theoretical predictions of analytical models are presented.



(a) Materials with only inclusion



(b) Materials with only pores



(c) Materials with both pores and inclusions

Figure 2.1-2 Variation of relative elastic modulus κ_{hom}/κ_s and μ_{hom}/μ_s with inclusion volume fraction and porosity for concrete materials.

As shown in Figure 2.1-3, we investigated the influence of these parameters on the macroscopic elastic properties of heterogeneous materials by considering microstructural parameters such as porosity, inclusion volume fraction, local elastic properties of the matrix phase, and inclusions. We

observed that for materials with high porosity or inclusion volume fraction, as well as for materials containing both pores and inclusions at the same scale, typical homogenization analytical models were unable to accurately predict their macroscopic elastic properties.

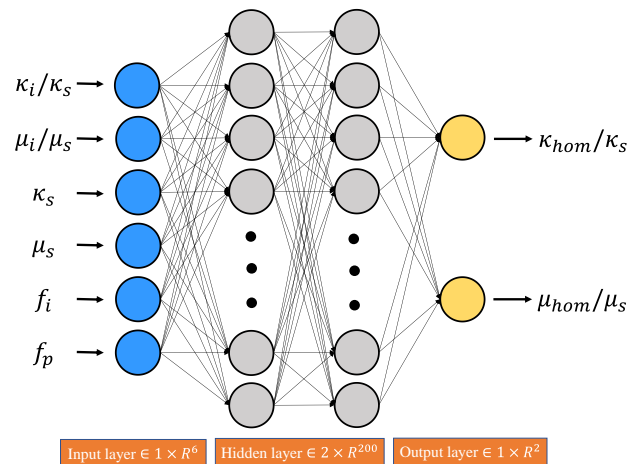
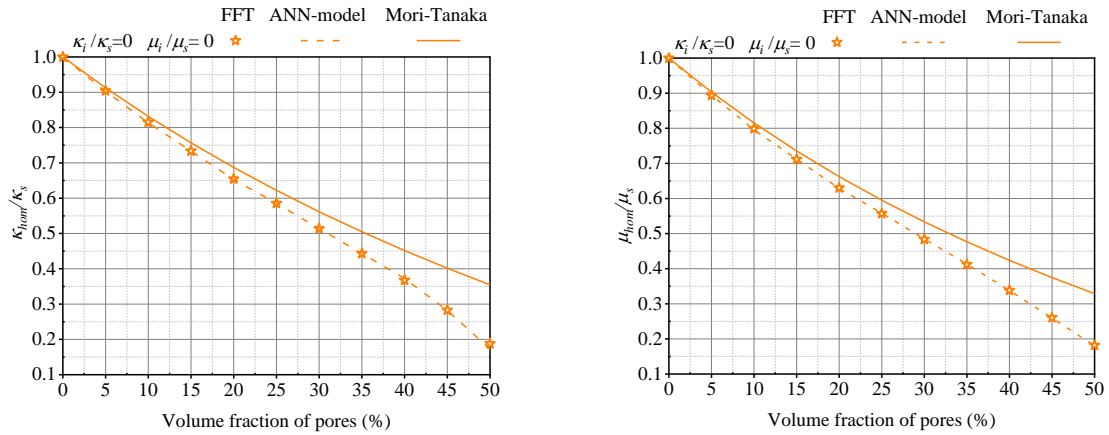
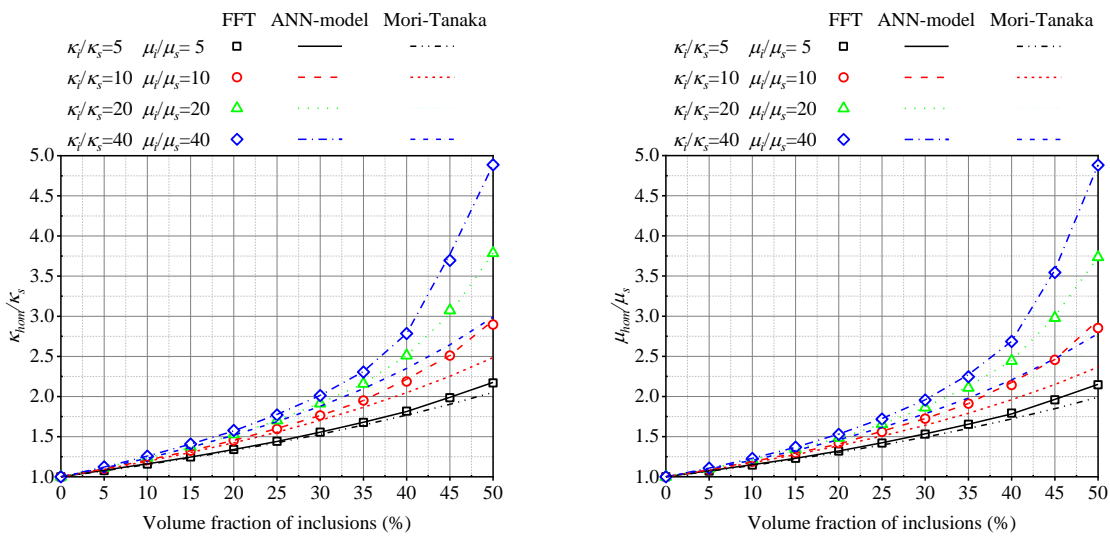


Figure 2.1-3 Artificial neural network structure for predicting effective elastic properties of concrete.

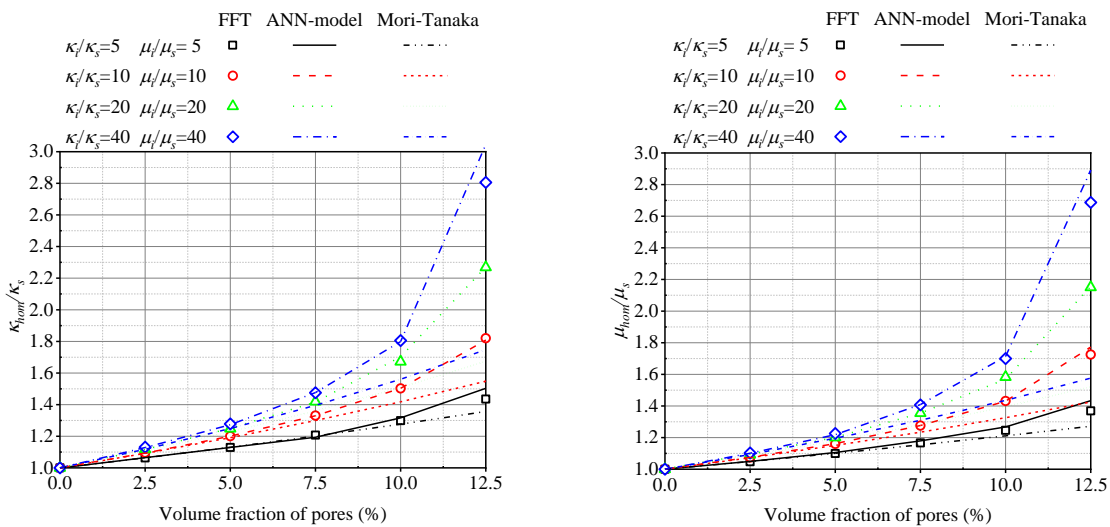
In light of this challenge, and with the aim of refining and enhancing these analytical predictions, we developed a model based on artificial neural networks (ANN). The structure of this model is illustrated in Figure 2.1-3. Following a rigorous process of training and testing using data derived from FFT simulation results, we discovered that this model exhibited exceptional levels of accuracy. Notably, the model demonstrated an exceedingly high R^2 value (greater than 0.999) and remarkably low RMSE and MAE values. Importantly, the predictive capabilities of the ANN-based model have significantly enhanced the accuracy of predictions compared to analytical models, as demonstrated in Figure 2.1-4.



(a) Materials with only inclusion



(b) Materials with only pores



(c) Materials with both pores and inclusions

Figure 2.1-4 Variations of normalized effective elastic moduli with porosity or inclusion fraction for different values of κ_i/κ_s and μ_i/μ_s for concrete materials.

2.1.4 Failure strength

In the past few decades, significant advancements have been made in understanding the nonlinear behaviour of heterogeneous materials. Particularly, various macroscopic strength criteria have been developed to assess the failure stresses of materials. However, establishing analytical strength criteria requires simplification of the microstructural morphology of concrete materials. For instance, attempting to derive analytical strength criteria by simultaneously considering pores, inclusions, and ITZ poses significant mathematical challenges, leading to the omission of ITZ effects in research studies. Based on these analyses, we considered an alternative matrix configuration involving inclusions, where the matrix contains pores at different scales, and the RVE of the material is illustrated in Figure 2.1-1. Dividing the material into three scales, the matrix of the material adheres to the Drucker-Prager criterion at the microscopic scale. By utilizing an improved secant method-based three-step nonlinear homogenization approach (Cao, Shen, Shao, & Wang, 2020, 2021; Maghous, Dormieux, & Barthelemy, 2009; Shen, Kondo, Dormieux, & Shao, 2013; Shen, Shao, Liu, Oueslati, & De Saxcé, 2020) the following closed-form expression for the macroscopic strength criterion can be derived:

$$F' = \frac{A' + \frac{2B'\rho}{3}}{1 + \frac{3\rho}{2} - \frac{5\rho}{6\left(\frac{A'}{B'} + 1\right)}} \Sigma_d^2 + B' \Sigma_m^2 + C' \Sigma_m - \left(D' + \frac{4B'D' + C'^2}{6A'} \rho \right) = 0 \quad 2.1-5$$

with the following coefficients:

$$A' = \frac{1}{T'^2} \left(\frac{6T'^2 - 6}{4T'^2 - 9} \phi + 1 \right), B' = \frac{3}{2T'^2} \phi - 1, \quad 2.1-6$$

$$C' = 2(1 - \phi)h', D' = (1 - \phi)^2 h'^2.$$

Where the parameters T' and h' denotes the frictional and cohesion coefficients of the porous cement paste at the microscopic scale.

Multi-scale models are developed for heterogeneous concrete materials to estimate their macroscopic mechanical properties in terms of micro-structural data. One crucial challenge of those models is the identification of local properties of constituent phases. To address this, we propose an effective method based on Artificial Neural Networks (ANN) for the identification of micro-level parameters in concrete. The primary goal is to determine the microscale frictional coefficient and cohesion of cement particles using macroscopic values of uniaxial compression and tensile strengths as inputs. By inverting the analytical strength criterion (as shown in Equation 2.1-7), a comprehensive dataset is constructed, incorporating aggregates volume fraction, porosity, macroscopic uniaxial tensile and compressive strengths as inputs, and the frictional coefficient and cohesion of cement particles as output unknowns.

$$\left(\frac{A' + \frac{2B'\rho}{3}}{1 + \frac{3\rho}{2} - \frac{5\rho}{6\left(\frac{A'}{B'} + 1\right)}} + \frac{B'}{9} \right) R^2 - \frac{C'}{3} R - \left(D' + \frac{4B'D' + C'^2}{6A'} \rho \right) = 0 \quad 2.1-7$$

An ANN model with four hidden layers, each containing 100 neurons (as depicted in Figure 2.1-5), is constructed and trained using this dataset. Multiple types of validation tests are performed for the ANN model. In Figure 2.1-6, the predicted values are plotted against the exact values to visualize their correlations. Remarkably high values of R^2 are achieved. These results highlight the effectiveness of

the proposed ANN-based model in accurately predicting the frictional coefficient and cohesion of porous cement paste at the microscopic scale.

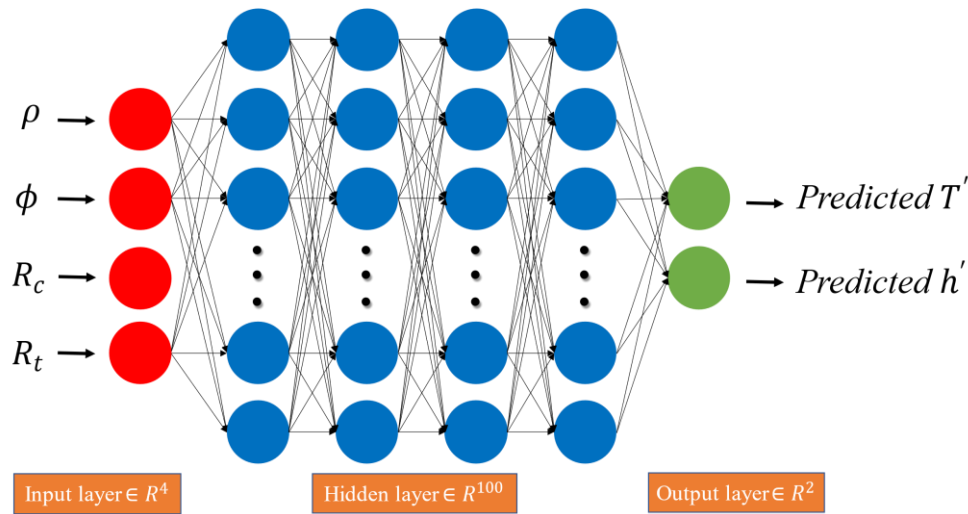


Figure 2.1-5 A BP neural network model to evaluate the microscopic parameter of concrete materials.

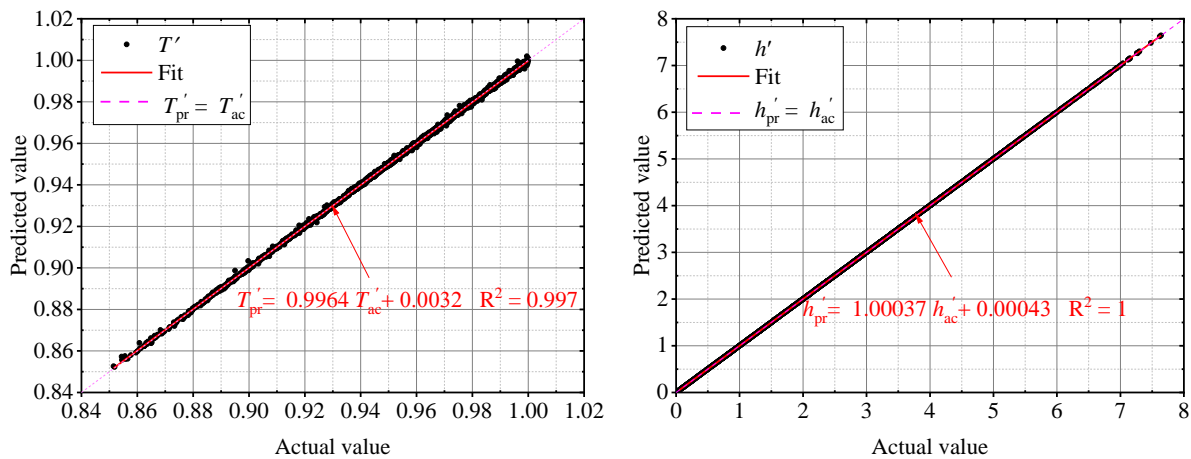


Figure 2.1-6 Correlation between predicted and exact values of T' and h' .

2.2 Other upscaling methods (led by CSIC)

2.2.1 Introduction

The aim of this section is to describe a methodology to assess the hydro-chemo-mechanical (HCM) behaviour of cementitious materials under repository conditions by developing predictive models from aggregate to the continuum scale (centimetres to meters, Figure 2.1-1). It should be noted that some of the subsections described are ongoing investigations or models that are in a conceptual stage.

First approach

To achieve the mentioned goal, it has been decided to define a hypothetical problem that simulates the interaction between a support (concrete) structure and the rock confining it in the long term and under repository conditions in a deep waste disposal. To quantify the potential effect of reaction-induced concrete degradation, it has been decided to address the problem separately: on the one hand, the hydro-mechanical problem; and on the other hand, the chemical problem. Finally, the idea is to couple both models into an HCM model that let us analyse the possible alteration on concrete and also, the behaviour of the surrounding rock.

EURAD Deliverable 16.8 – MAGIC - S/T 4-1 – 4/2 -Chemo-mechanical numerical coupling development and up-scaling methods

The following sections describe the codes and software that have been used to elaborate these models, a description of their dimensions and parameters and some preliminary results, for those at more advanced stages of work.

2.2.2 Hydro-Mechanical model

An elastic model of the hydro-mechanical (Schloegl, Schmidt, Boeckle, Weiss, & Kotschal) response of a concrete support structure and the surrounding rock under repository conditions has been built. CODE_BRIGHT has been selected to develop the model and analyse the behaviour of both materials. The model has allowed us to numerically observe deformations, variation in porosity and stresses. Preliminary results will be described and discussed in the following sections.

2.2.2.1 CODE_BRIGHT

CODE_BRIGHT (COupled DEformation of BRIne Gas and Heat Transport) is a finite element method (FEM) program designed and capable to perform fully coupled thermo-hydro-mechanical (THM) problems in geological media (S. Olivella, Gens, Carrera, & Alonso, 1996). CODE_BRIGHT (https://deca.upc.edu/en/projects/code_bright) is an open access code that has been developed at the Department of Civil and Environmental Engineering at the Technical University of Catalonia (UPC), and works combined with the pre/post-processor GiD (<https://www.gidsimulation.com/>), developed by the International Center for Numerical Methods in Engineering (CIMNE).

GiD is an interactive graphical user interface that is used for definition, preparation and visualisation of all the data related to numerical simulations. The theoretical approach consists in a set of governing equations, a set of constitutive laws and a special computational approach. The code is written in FORTRAN and it is composed by several subroutines.

In general, the complete solution process can be described as: i) the definition of the geometry of the problem, ii) the definition of attributes and conditions, iii) the creation of a mesh, iv) the computing processes that perform the simulations and v) the post-process that allows to visualize and interpret the results. The geometrical domain is based on four geometrical levels entities (points, lines, surfaces and volumes), all of them considered in a three-dimensional space.

2.2.2.2 Model description

The objective of the HM model is to know the evolution of deformations and state of stresses in the support structure of a disposal facility, as well as in the surrounding rock of the medium, in the long term. In this stage of the research, the aim is to define the dimensions and the environment where different simulations will be carried out. It is also important to know the porosity variations in each material considering only the geomechanically effect. By doing so, it is defined the groundwork where at a later stage the chemical effect in materials will be coupled into a HCM model.

Four stages are defined for the creation of the HM model. First, an early simple model is created to gathers all the mechanical and hydraulic parameters that allow the system to reach the steady state. Since the disposal facility is defined as an underground cavity, the second stage consists in designing an excavation sequence and determine the alterations caused in the medium during the drilling. Third, a support structure is constructed as a lining of the cavity. Lastly, the fourth stage consists in evaluating the behaviour of the entire system in the long term. Each of the mentioned stages requires to compute a new equilibrium state prior to moving to the next one. The time intervals of each stage are 200 days to reach the initial steady state, i.e., the equilibration stage, 7 days of excavation, 1 day to construct the support structure and 9,125 days of evaluation period, equivalent to 25 years of analysis. This HM model is referred as the “base model”.

To test the potential effect of concrete alteration, the area of the support structure that directly interacts with the rock, at the concrete rock interface, we change the mechanical properties of the 5 cm of concrete that are closer to the rock. The aim is to observe the effect over the system of a weakened

material, considering that in the future it is intended to couple the chemical effect to the problem. For disclosure and comparison purposes, this test model is called “altered model”.

2.2.2.3 Model parameters

Considerations. The simulations performed in a first approach of the problem are carried out into an elastic, homogeneous and isothermal medium. It is planned to use other characteristics of the environment in future modelling, like considering a viscoplastic behaviour of the rock.

It should be mentioned that in the long term under repository conditions, it is expected that chemical reactions take place and potentially lead to changes in hydraulic properties (i.e., porosity and permeability) and/or geomechanical properties (i.e., stiffness and strength) (Vilarrasa, Makhnenko, & Rutqvist, 2019). Due to the contrasting chemical and mineralogical properties of cementitious materials and rocks (in this particular case for clay formation), interactions will occur at the cement-rock interface as a result of the chemical gradients (Deissmann, 2021). These HM models do not include directly the chemical effect, therefore, to perform tests on the model, it has been determined to increase the porosity of a defined zone of the concrete support structure and at the same time, decrease the Young’s modulus in this selected area.

Dimensions and boundary conditions. Two-dimensional modelling has been performed. The Figure 2.2-1 shows a graphical representation of the geometry of the model performed.

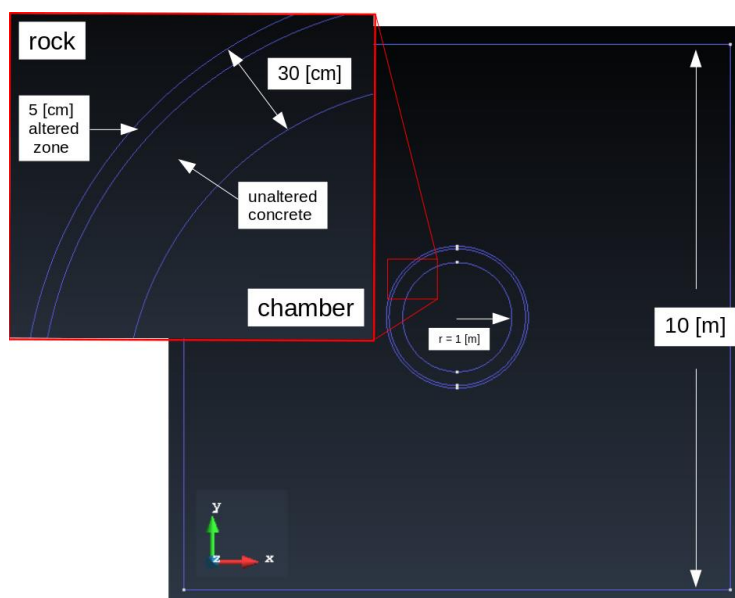


Figure 2.2-1: 2D HM model dimensions.

The model is a square that extends 10 m in the vertical and horizontal directions. In the center, the cavity that acts as disposal facility is represented as a circle to model a circular tunnel. Figure 2.2-1 shows three concentric circles, each of them representing different steps during modelling. The external circle represents the excavation with a radius of 1.30 m; the inner circle represents the delimitation of the disposal chamber of 1.00 m in radius. The spacing defined by the subtraction between the external and inner circles areas corresponds to the concrete support structure of 0.30 m thick. There is a circle with a radius of 1.25 m, which purpose is to demarcate the limit of the concrete with unaltered characteristics and the other whose properties are degraded by chemical reactions. In the “base model”, it is considered the entire 0.30 m thick area as unaltered concrete, while the “altered model” considers a 0.25-m thick area of unaltered concrete and a 0.05-m thick external area with weakened concrete.

It is assumed that the disposal facility is located at 500-m depth. As mechanical boundary conditions, a lithostatic load of 12 MPa is placed on the top boundary of the model. Displacement is impeded in the direction perpendicular to the boundary in the other boundaries. As flux boundary conditions, a 5 MPa

liquid pressure is set at the bottom boundary, while no-flux condition is imposed on the other borders. The flux boundary condition of the circles depends on the stage of modelling. During the steady-state stage there are no conditions; after the excavation, the system allows flux at the external 1.30 m radius circle by prescribing atmospheric pressure on it; and after the construction of the concrete support, this condition is set at the inner 1.00-m radius circle.

Material properties and meshing. The mechanical and hydraulic rock properties are based on measured laboratory results reported by (Kim, Vilarrasa, & Makhnenko, 2018). Moreover, the concrete properties are based on reported data by (S. Olivella, Vaunat, J., Rodriguez-Dono, A. , 2021). For the weakened concrete in the concrete-rock interface of the “altered model”, an increased porosity and 30% decreased Young’s modulus is imposed. Table 2.2-1 listed the used material properties.

Table 2.2-1 Material properties (HM process).

Properties	Rock	Concrete	Altered zone
Young’s Modulus [MPa]	5000	30000	21000
Poisson’s ratio	0.3	0.2	0.2
Porosity	0.10	0.15	0.25
Permeability [m ²]	1E-20	1E-19	1E-19

A structured quadrilateral element type mesh is selected and generated to solve the model. The element size depends on the proximity to the concrete support. The minimum element size is 0.02 m and constitutes the concrete support structure and the surrounding rock. The maximum element size is 1 m and is located at the boundaries. This guarantees accurate results in the main area of interest, which is the concrete-rock interface, and relieves the calculation process, making it more efficient. Furthermore, information about the model is that it has 10,293 elements, 9,586 nodes and takes around 27 hours to complete the processing period.

2.2.2.4 Preliminary results

Due to the symmetry of the problem, 12 points were analysed per model; 6 on a vertical section and 6 on a horizontal one. The selected evaluation points were located within the support structure and at different distances away from the support into the host rock, as show in Figure 2.2-2. The evolution of deformations, porosity, stresses in x, y and z directions (σ_x , σ_y & σ_z), the shear stress in the x-y plane (τ_{xy}), and the liquid pressure P_L is evaluate in each of these points.

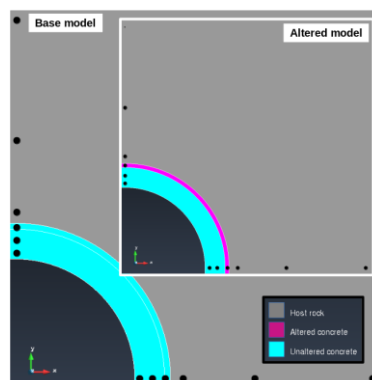


Figure 2.2-2: Analysed points.

Two mm deformations are observed in the vertical section within the support structure. In the horizontal section, the deformations observed have a magnitude of 0.8 mm. Similar values are observed in both “base” and “altered” model. In relation with the variation of porosity of the concrete structure due to

geomechanically effect, it is observed that this parameter remains invariable in the evaluated period of 25 years.

With the liquid pressure information and the stresses result data, the mean effective stress p' and the deviatoric stress q have been calculated to plot the stress path of each analysed point and compare differences between “base” and “altered” models. Figure 2.2-3 presents the stress paths within the concrete support structure and Figure 2.2-4 at different distances away into the host rock.

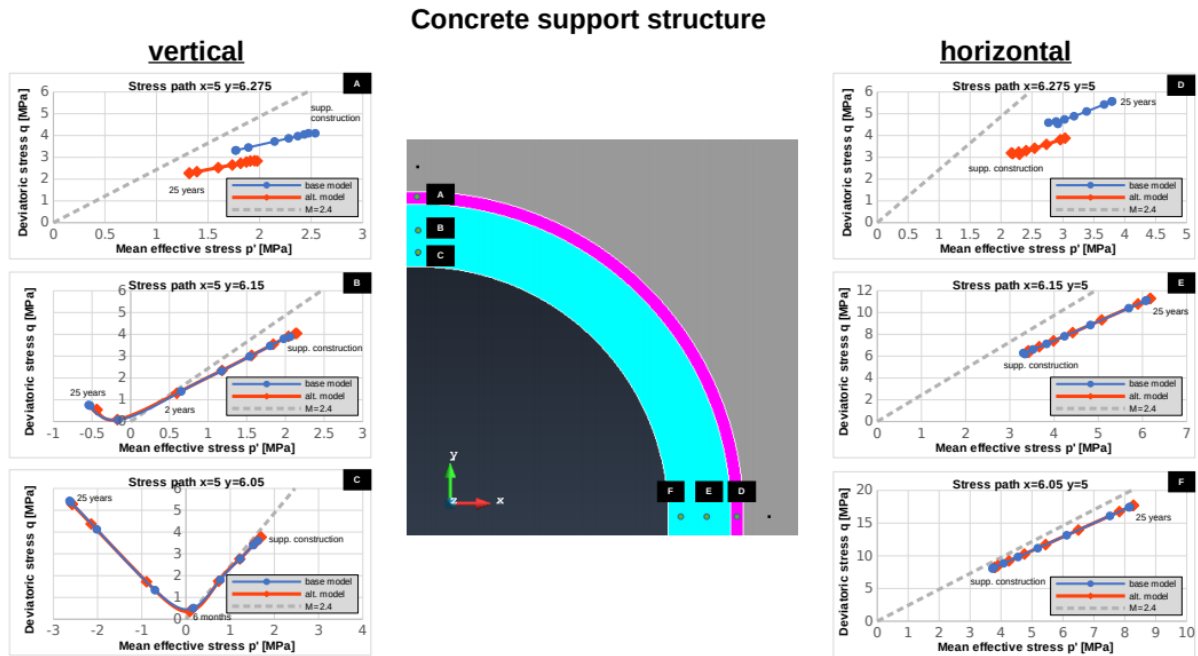


Figure 2.2-3: Stress path of concrete in the analysed points.

In the vertical section of the concrete structure, it is observed that the state of stress is under compression during the 25-year period of simulation and the stress path at point A is below the failure limit in both “base” and “altered” models (Figure 2.2-3). As long as it is analysed closer to the inner area of the lining, the failure limit is exceeded and the stress state changes from compression to tension. Point B reaches failure after 2 years, while point C reaches it after 6 months. On the horizontal section, all support structure points are in a compression stress state and remain below the failure limit during the whole evaluated period.

In the vertical section of the rock, it is observed that the distant points from the excavation (G and H) present stress paths in a compression stress regime and below the failure limit for both models (Figure 2.2-4). In contrast, the closest point to the excavated zone shows a stress path that is located above the failure limit since the beginning of the simulation. In the horizontal section, it is observed that all points follow a stress path that exceed the failure limit. It can be inferred with these mechanical observations that an excavation damage zone is observed in the surrounding area of excavation and this zone extends at least 10 cm above the excavation vertically and 2 m away horizontally (not included in the base model yet).

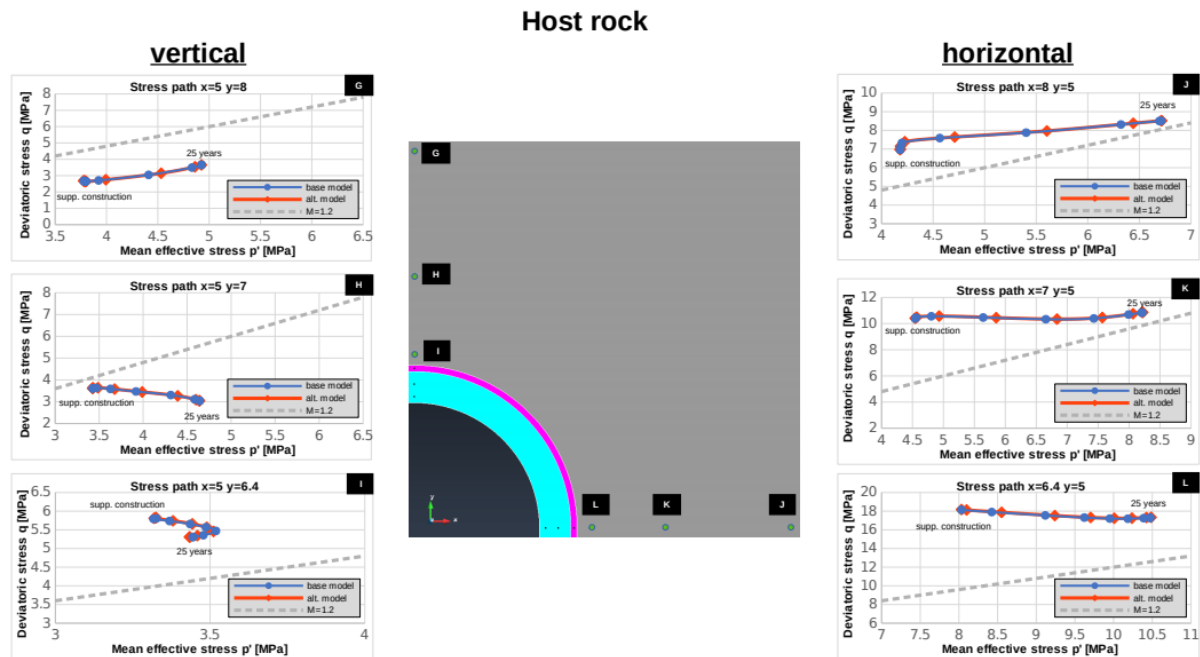


Figure 2.2-4: Stress path of rock analysed points

2.2.2.5 Future work

Tests are being performed to incorporate a viscoplasticity (Drucker-Prager) constitutive approach into the model. At a testing stage, it has been achieved to incorporate this model on the concrete support structure, maintaining a linear elastic constitutive model in the host rock. Efforts are being made in order to accomplish incorporating this approach in both materials within a single model.

Finally, and as mentioned above, the last phase of modelling will be achieved when the chemical effect is coupled into a HCM model, what will be done after the chemical model is made. The status of this phase is commented in the following section.

2.2.3 Chemical modelling

We perform reactive transport modelling of the concrete-rock chemical system to address this stage of the work. Retraso-CODE_BRIGHT has been selected to elaborate and evaluate the precipitation or dissolution of species in the concrete-rock interface, which could lead to variation in porosity in either concrete or rock materials. A brief overview of the code to be used and the model to be performed are described below.

2.2.3.1 Retraso-CODE_BRIGHT

The code Retraso-CODE_BRIGHT (RCB) is designed to model complex problems consisting of coupled thermal, hydraulic and geochemical processes. It is developed by the Hydrogeology Research Group (GHS) from the Department of Civil Engineering at the Technical University of Catalonia (UPC), in collaboration with the Institute of Environmental Assessment and Water Research (IDAEA), Spanish National Research Council (CSIC), in Barcelona, Spain.

Some of the tasks that can be performed are simulations of the flow of liquid and/or gas in a multi-phase approach; simulations of transport (advection, dispersion and diffusion) of chemical species in the liquid and gas phase; simulations of chemical reactions like aqueous complexation, including redox and acid-base reactions; sorption, including cation exchange; precipitation and dissolution of minerals, those can be considered kinetically or in equilibrium; the effects of precipitation and dissolution on porosity and permeability; and many others, considering using one, two or three-dimensional finite elements for its

EURAD Deliverable 16.8 – MAGIC - S/T 4-1 – 4/2 -Chemo-mechanical numerical coupling development and up-scaling methods

spatial discretization in a user friendly graphic interface that can be used in both pre- and post-processing of the data.

RCB is the result of coupling two codes: the already mentioned CODE_BRIGTH, which is designed for the thermo-hydro-mechanical analysis of three-dimensional multiphase saline media (S. Olivella et al., 1996) and Retraso (REactive TRAnsport of Solutes), which, as mentioned, is a code for solving 1D, 2D or 3D reactive transport problems (Saaltink, 1997). Basically, in the coupled code RCB, a CODE_BRIGTH module calculates the flow properties (i.e., Darcy flux of liquid and/or gas, saturation, temperature, density, etc.) and passes it to a Retraso module for the calculation of reactive transport. At this stage, RCB does not solve the mechanical problem (i.e., stresses, deformations, etc.) in CODE_BRIGTH.

2.2.3.2 Model description

To simulate the interaction between concrete and rock, a simple one-dimensional model is performed. The idea is to consider the main species that could react from concrete and thus are related to the variation on porosity, according to the results observed in different studies (Kangni-Foli et al., 2021; Soler, 2022). Then, the system must be allowed to react to achieve that reactants and products are consistent with the problem to be solve.

In future chemical models, the precipitation of secondary species in the rock side of the problem will be considered, and therefore, a more complete and complex chemical system in each concrete and surrounding rock.

2.2.3.3 Model parameters

Considerations

Since the elaboration of this model requires a source of input information and there is not any ongoing experiment or rather, a large amount of experimental data, different sources have been chosen to create a model, an with it evaluate the evolution of the chemical system.

The studies conducted at the Mont Terri Underground Rock Laboratory have been considered, in particular, those related to the Cement-Clay Interaction (CI and CI-D) experiment (Mäder et al. 2018). The results of the experiment, as well as previous studies that lay the groundwork for the development of reactive transport models, are to be used as basis for the development of this first simulation. As assumed in the HM model, the material defining the concrete support structure is characterized by Portland cement and the rock characteristics come from Opalinus Clay formation.

It is expected in the next few months that experimental information will be available into MAGIC's Interactive Database of Cement Properties (IDCP), to calibrate and validate our model or even create new models with new data related to relevant experiments.

Dimensions

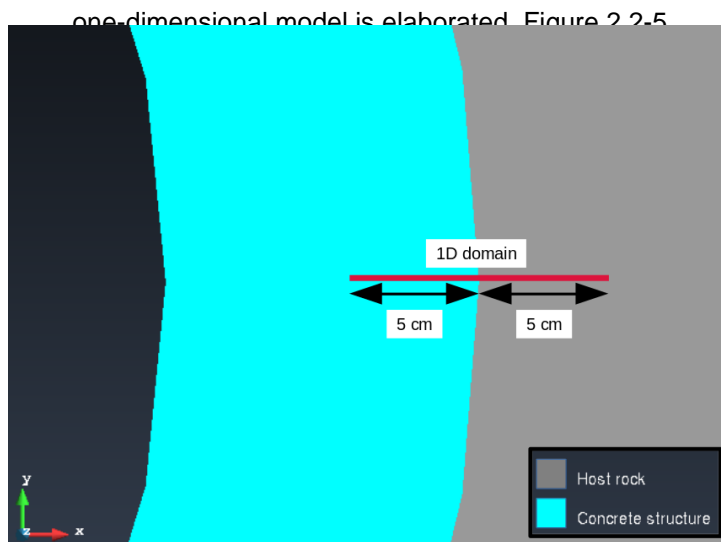


Figure 2.2-5 shows a scheme of the geometry of the model. The considered section for this problem includes 5 cm of concrete and 5 cm of rock, thus, the length of the model will be 10 cm. All domain boundaries are considered to have a no-flux condition.

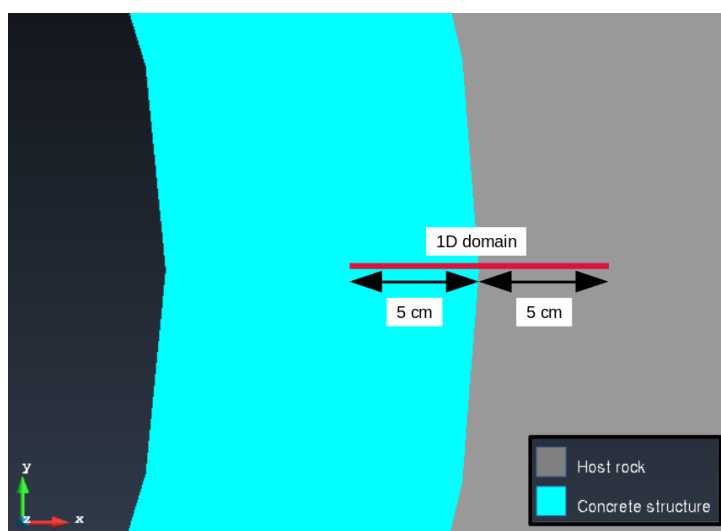


Figure 2.2-5: 1D domain for the chemical model

Composition of concrete and rock

The initial composition of the concrete is simplified to consider only portlandite, calcium-silicate-hydrate (C-S-H) minerals and quartz as the aggregate, in this first instance. Initially, only the changes on the concrete side will be evaluated. At this stage, the rock will be assumed to be composed only of calcite. Table 1.2-1 shows the initial composition selected for each mineral species.

Table 2.2-2: Initial composition of concrete and rock for calculations.

Material	Mineral	Vol. fr.	A [m ² /m ³]
Concrete	CSH	0.091	10 ⁴
	Portlandite	0.046	10 ⁴
	Quartz	0.725	4.68x10 ²
	Porosity	0.138	-----
Rock	Calcite	0.850	1.03x10 ⁵
	Porosity	0.150	-----

where $A [m^2/m^2]$ is the specific surface available to reactive processes

The composition of concrete for the calculations is based on Lothenbach et al. (B. Lothenbach, 2011B) and the composition of rock on Jenni et al. (2017), adapted for this simplified problem. The reactive surface areas and porosity are based on Soler et al. (Soler, 2022).

Solution composition

The initial composition of the rock porewater is based on the composition reported by (Mäder et al., 2018), Mäder (2018) and the initial concrete porewater is based on Lothenbach (2011b) for fully hydrated cement and equilibrated with the initial cement phases. For both porewaters, the considered ions are adapted for this simple model. Table 2.2-3 shows the compositions involved in this model.

Table 2.2-3 Initial composition (total molalities) of concrete and rock porewaters. Equilibrium and charge balance constraints are indicated in parentheses.

Parameter	Concrete	Rock
Na ⁺	9.00x10 ⁻¹	2.37x10 ⁻¹ (charge)
K ⁺	2.09x10 ⁻¹	1.43x10 ⁻³
Ca ²⁺	2.49x10 ⁻³ (portlandite)	1.52x10 ⁻²
Cl ⁻	1.00x10 ⁻⁸	2.72x10 ⁻¹
SiO ₂ (aq)	5.87x10 ⁻⁵ (CSH)	1.32x10 ⁻⁴
HCO ₃ ⁻	8.28x10 ⁻⁵ (calcite)	1.47x10 ⁻³ (calcite)
T [°C]	15	15
pH	13.63 (charge)	7.50

The composition of concrete porewater is consistent with the mineral species that constitute this material. Similarly, the composition of rock porewater is in equilibrium with the initial mineral composition of the rock. This condition guarantee that the porewater in each material does not react with the medium and that chemical reactions that take place occur at the concrete-rock interface, due to the different composition between both initial porewaters.

Future work and parameters to define

The development of this model is at a conceptual stage, therefore, there are still parameters to be defined properly for solutions and solid phase reactions (activity coefficients, equilibrium constants, others). Once the different pieces of the coupling work independently, RCB will be used to solve the coupled HMC problem. The chemically-induced concrete degradation will need to be upscaled from aggregate to continuum scale. This upscaling will be done in collaboration with UFZ and the idea is to use upscaling laws that correlate porosity variations with Young's modulus changes.

Final model results will be presented in deliverable D16.9.

REFERENCES

- Bary, B., & Sellier, A. (2004). Coupled moisture—carbon dioxide—calcium transfer model for carbonation of concrete. *Cement and Concrete Research*, 34(10), 1859-1872.
- Bilke, L., Flemisch, B., Kalbacher, T., Kolditz, O., Helmig, R., & Nagel, T. (2019). Development of open-source porous media simulators: principles and experiences. *Transport in porous media*, 130, 337-361.
- Biot, M. A. (1941). General theory of three-dimensional consolidation. *Journal of applied physics*, 12(2), 155-164.
- Bourdin, B., Francfort, G. A., & Marigo, J.-J. (2008). The variational approach to fracture. *Journal of elasticity*, 91, 5-148.
- Cao, Y., Shen, W., Shao, J.-F., & Wang, W. (2020). A novel FFT-based phase field model for damage and cracking behavior of heterogeneous materials. *International Journal of Plasticity*, 133, 102786.
- Cao, Y., Shen, W., Shao, J.-F., & Wang, W. (2021). A multi-scale model of plasticity and damage for rock-like materials with pores and inclusions. *International Journal of Rock Mechanics and Mining Sciences*, 138, 104579.
- Churakov, S. V., & Prasianakis, N. I. (2018). Review of the current status and challenges for a holistic process-based description of mass transport and mineral reactivity in porous media. *American Journal of Science*, 318(9), 921. doi:10.2475/09.2018.03
- Dauzères, A. (2016). Geochemical and physical evolution of cementitious materials in an aggressive environment. In T. Vehmas & E. Holt (Eds.), *CEBAMA - WP1 Experimental studies – State of the art literature review* (Vol. D 1.03).
- Dauzères, A., Helson, O., Churakov, S., Montoya, V., Zghondi, J., Neeft, E., . . . Vilarrasa, V. (2022). *MAGIC - T1 - Initial State of the Art on the chemo-mechanical evolution of cementitious materials in disposal conditions : EURAD D16.1*.
- De Graef, B., Cnudde V Fau - Dick, J., Dick J Fau - De Belie, N., De Belie N Fau - Jacobs, P., Jacobs P Fau - Verstraete, W., & Verstraete, W. (2005). A sensitivity study for the visualisation of bacterial weathering of concrete and stone with computerised X-ray microtomography. (0048-9697 (Print)).
- Deissmann, G., Ait Mouheb, N., Martin, C., Turrero, M. J., Torres, E., Kursten, B., Weetjens, E., Jacques, D., Cuevas, J., Samper, J., Montenegro, L., Leivo, M., Somervouri, M., Carpen, L. . (2021). *Experiments and numerical model studies interfaces*. Retrieved from
- Francfort, G. A., & Marigo, J.-J. (1998). Revisiting brittle fracture as an energy minimization problem. *Journal of the Mechanics and Physics of Solids*, 46(8), 1319-1342.
- Galan, I., Glasser, F. P., Baza, D., & Andrade, C. (2015). Assessment of the protective effect of carbonation on portlandite crystals. *Cement and Concrete Research*, 74, 68-77. doi:<https://doi.org/10.1016/j.cemconres.2015.04.001>
- Gerard, B., Pijaudier-Cabot, G., & Laborderie, C. (1998). Coupled diffusion-damage modelling and the implications on failure due to strain localisation. *International Journal of Solids and Structures*, 35(31-32), 4107-4120.
- Gong, F., Zhang, D., Sicat, E., & Ueda, T. (2014). Empirical Estimation of Pore Size Distribution in Cement, Mortar, and Concrete. *Journal of Materials in Civil Engineering*, 26(7), 04014023. doi:10.1061/(ASCE)MT.1943-5533.0000945
- Griffith, A. A. (1921). VI. The phenomena of rupture and flow in solids. *Philosophical transactions of the royal society of london. Series A, containing papers of a mathematical or physical character*, 221(582-593), 163-198.
- Huang, H., Sukop, M. C., & Lu, X.-Y. (2015). *Multiphase Lattice Boltzmann Methods: Theory and Application*: John Wiley & Sons, Ltd.

EURAD Deliverable 16.8 – MAGIC - S/T 4-1 – 4/2 -Chemo-mechanical numerical coupling development and up-scaling methods

- Huang, Y., Shao, H., Wieland, E., Kolditz, O., & Kosakowski, G. (2018). A new approach to coupled two-phase reactive transport simulation for long-term degradation of concrete. *Construction and Building Materials*, 190, 805-829. doi:<https://doi.org/10.1016/j.conbuildmat.2018.09.114>
- Ishida, T., & Maekawa, K. (2000). Modeling of pH profile in pore water based on mass transport and chemical equilibrium theory. *Doboku Gakkai Ronbunshu*, 2000(648), 203-215.
- Jain, A. K., Jianchang, M., & Mohiuddin, K. M. (1996). Artificial neural networks: a tutorial. *Computer*, 29(3), 31-44. doi:10.1109/2.485891
- Johannsen, K., & Rademacher, S. (1999). Modelling the Kinetics of Calcium Hydroxide Dissolution in Water. *Acta hydrochimica et hydrobiologica*, 27(2), 72-78. doi:[https://doi.org/10.1002/\(SICI\)1521-401X\(199902\)27:2<72::AID-AHEH72>3.0.CO;2-H](https://doi.org/10.1002/(SICI)1521-401X(199902)27:2<72::AID-AHEH72>3.0.CO;2-H)
- Jourdain, X. (2014). *Etude numérique méso-macro des propriétés de transfert des bétons fissurés*. Ecole normale supérieure de Cachan-ENS Cachan,
- Kangni-Foli, E., Poyet, S., Le Bescop, P., Charpentier, T., Bernachy-Barbé, F., Dauzères, A., . . . de Lacaillerie, J.-B. d. E. (2021). Carbonation of model cement pastes: The mineralogical origin of microstructural changes and shrinkage. *Cement and Concrete Research*, 144, 106446.
- Kim, K., Vilarrasa, V., & Makhnenko, R. Y. (2018). CO₂ injection effect on geomechanical and flow properties of calcite-rich reservoirs. *Fluids*, 3(3), 66.
- Kulik, D. A., Wagner, T., Dmytrieva, S. V., Kosakowski, G., Hingerl, F. F., Chudnenko, K. V., & Berner, U. R. (2013). GEM-Selektor geochemical modeling package: revised algorithm and GEMS3K numerical kernel for coupled simulation codes. *Computational Geosciences*, 17(1), 1-24. doi:10.1007/s10596-012-9310-6
- Kuznik, F., Obrecht, C., Rusaouen, G., & Roux, J.-J. (2010). LBM based flow simulation using GPU computing processor. *Computers & Mathematics with Applications*, 59(7), 2380-2392. doi:<https://doi.org/10.1016/j.camwa.2009.08.052>
- Lallemand, P., & Luo, L.-S. (2000). Theory of the lattice Boltzmann method: Dispersion, dissipation, isotropy, Galilean invariance, and stability. *Physical Review E*, 61(6), 6546-6562. doi:10.1103/PhysRevE.61.6546
- Laloy, E., & Jacques, D. (2022). Speeding Up Reactive Transport Simulations in Cement Systems by Surrogate Geochemical Modeling: Deep Neural Networks and k-Nearest Neighbors. *Transport in Porous Media*, 143(2), 433-462. doi:10.1007/s11242-022-01779-3
- Lasaga, A. C. (2014). *Kinetic Theory in the Earth Sciences*: Princeton University Press.
- Lothenbach, B. (2011B). *CI Experiment: Hydration experiments of OPC, LAC AND ESDRED cements: 1 h to 3.5 years*. Retrieved from
- Lothenbach, B., & Winnefeld, F. (2006). Thermodynamic modelling of the hydration of Portland cement. *Cement and Concrete Research*, 36(2), 209-226. doi:<https://doi.org/10.1016/j.cemconres.2005.03.001>
- Lu, R., Nagel, T., Poonosamy, J., Naumov, D., Fischer, T., Montoya, V., . . . Shao, H. (2022). A new operator-splitting finite element scheme for reactive transport modeling in saturated porous media. *Computers & Geosciences*, 163, 105106.
- Mäder, U., Jenni, A., Lerouge, C., Gaboreau, S., Miyoshi, S., Kimura, Y., . . . Lothenbach, B. (2018). 5-year chemico-physical evolution of concrete–claystone interfaces, Mont Terri rock laboratory (Switzerland). In P. Bossart & A. G. Milnes (Eds.), *Mont Terri Rock Laboratory, 20 Years: Two Decades of Research and Experimentation on Claystones for Geological Disposal of Radioactive Waste* (pp. 309-329). Cham: Springer International Publishing.
- Mäder, U., Jenni, A., Lerouge, C. et al. 5-year chemico-physical evolution of concrete–claystone interfaces, Mont Terri rock laboratory (Switzerland). *Swiss J Geosci* 110, 307–327 (2017). <https://doi.org/10.1007/s00015-016-0240-5>
- Maghous, S., Dormieux, L., & Barthelemy, J. (2009). Micromechanical approach to the strength properties of frictional geomaterials. *European Journal of Mechanics-A/Solids*, 28(1), 179-188.

EURAD Deliverable 16.8 – MAGIC - S/T 4-1 – 4/2 -Chemo-mechanical numerical coupling development and up-scaling methods

- Matallah, M., La Borderie, C., & Maurel, O. (2010). A practical method to estimate crack openings in concrete structures. *International Journal for Numerical and Analytical Methods in Geomechanics*, 34(15), 1615-1633.
- Nilenius, F., Larsson, F., Lundgren, K., & Runesson, K. (2015). Mesoscale modelling of crack-induced diffusivity in concrete. *Computational Mechanics*, 55, 359-370.
- Olivella, S., Gens, A., Carrera, J., & Alonso, E. (1996). Numerical formulation for a simulator (CODE_BRIGHT) for the coupled analysis of saline media. *Engineering computations*, 13(7), 87-112.
- Olivella, S., Vaunat, J., Rodriguez-Dono, A. . (2021). *CODE_BRIGHT 2021 Tutorial Manual. VIII. Tutorial example: Sequential Excavation Method - SEM.*: Universitat Politècnica de Catalunya. Department of Civil and Environmental Engineering.
- Parkhurst, D. L. (1995). *User's guide to PHREEQC, a computer program for speciation, reaction-path, advective-transport, and inverse geochemical calculations* (95-4227). Retrieved from Reston, VA: <http://pubs.er.usgs.gov/publication/wri954227>
- Patel, R. A., Churakov, S. V., & Prasianakis, N. I. (2021). A multi-level pore scale reactive transport model for the investigation of combined leaching and carbonation of cement paste. *Cement and Concrete Composites*, 115, 103831. doi:<https://doi.org/10.1016/j.cemconcomp.2020.103831>
- Patel, R. A., Perko, J., Jacques, D., De Schutter, G., Van Breugel, K., & Ye, G. (2014). A versatile pore-scale multicomponent reactive transport approach based on lattice Boltzmann method: Application to portlandite dissolution. *Physics and Chemistry of the Earth*, 70-71, 127-137. doi:10.1016/j.pce.2014.03.001
- Patel, R. A., Perko, J., Jacques, D., De Schutter, G., Ye, G., & Van Breugel, K. (2018). A three-dimensional lattice Boltzmann method based reactive transport model to simulate changes in cement paste microstructure due to calcium leaching. *Construction and Building Materials*, 166, 158-170. doi:10.1016/j.conbuildmat.2018.01.114
- Peycelon, H., Blanc, C., & Mazoin, C. (2006). Long-term behaviour of concrete: Influence of temperature and cement binders on the degradation (decalcification/hydrolysis) in saturated conditions. *Revue européenne de génie civil*, 10(9), 1107-1125.
- Phung, Q. T., Maes, N., Jacques, D., De Schutter, G., Ye, G., & Perko, J. (2016). Modelling the carbonation of cement pastes under a CO₂ pressure gradient considering both diffusive and convective transport. *Construction and Building Materials*, 114, 333-351. doi:<https://doi.org/10.1016/j.conbuildmat.2016.03.191>
- Prasianakis, N. I., Curti, E., Kosakowski, G., Poonoosamy, J., & Churakov, S. V. (2017). Deciphering pore-level precipitation mechanisms. *Scientific Reports*, 7. doi:ARTN 13765
10.1038/s41598-017-14142-0
- Prasianakis, N. I., Gatschet, M., Abbasi, A., & Churakov, S. V. (2018). Upscaling Strategies of Porosity-Permeability Correlations in Reacting Environments from Pore-Scale Simulations. *Geofluids*. doi:Unsp 9260603
10.1155/2018/9260603
- Prasianakis, N. I., Haller, R., Mahrous, M., Poonoosamy, J., Pflingsten, W., & Churakov, S. V. (2020). Neural network based process coupling and parameter upscaling in reactive transport simulations. *Geochimica Et Cosmochimica Acta*, 291, 126-143. doi:10.1016/j.gca.2020.07.019
- Qian, Y.-H., d'Humières, D., & Lallemand, P. (1992). Lattice BGK models for Navier-Stokes equation. *EPL (Europhysics Letters)*, 17(6), 479.
- Rumelhart, D. E., Hinton, G. E., & Williams, R. J. (1986). Learning representations by back-propagating errors. *Nature*, 323(6088), 533-536. doi:10.1038/323533a0
- Saaltink, M., Benet, I., Ayora, C. . (1997). *RETRASO, Fortran Code for Solving 2D Reactive Transport of Solutes, User's guide.* : Departamento de Ingeniería del Terreno, Universitat Politècnica de Catalunya and Instituto de Ciencias de la Tierra, CSIC, Barcelona.

EURAD Deliverable 16.8 – MAGIC - S/T 4-1 – 4/2 -Chemo-mechanical numerical coupling development and up-scaling methods

- Safi, M. A., Prasianakis, N., & Turek, S. (2017). Benchmark computations for 3D two-phase flows: A coupled lattice Boltzmann-level set study. *Computers & Mathematics with Applications*, 73(3), 520-536. doi:10.1016/j.camwa.2016.12.014
- Savage, D., & Cloet, V. (2018). *A review of Cement-Clay Modelling*. Retrieved from
- Schloegl, C., Schmidt, J., Boeckle, M., Weiss, B. M., & Kotschal, K. (2012). Grey parrots use inferential reasoning based on acoustic cues alone. *Proceedings of the Royal Society B-Biological Sciences*, 279(1745), 4135-4142. doi:10.1098/rspb.2012.1292
- Schmidt, T., Lothenbach, B., Romer, M., Neuenschwander, J., & Scrivener, K. (2009). Physical and microstructural aspects of sulfate attack on ordinary and limestone blended Portland cements. *Cement and Concrete Research*, 39(12), 1111-1121. doi:<https://doi.org/10.1016/j.cemconres.2009.08.005>
- Schuler, L., Ilgen, A. G., & Newell, P. (2020). Chemo-mechanical phase-field modeling of dissolution-assisted fracture. *Computer Methods in Applied Mechanics and Engineering*, 362, 112838.
- Seigneur, N., De Windt, L., Déjeant, A., Lagneau, V., & Descostes, M. (2021). Long-term evolution of uranium mobility within sulfated mill tailings in arid regions: a reactive transport study. *Minerals*, 11(11), 1201.
- Seigneur, N., De Windt, L., Poyet, S., Socié, A., & Dauzères, A. (2022). Modelling of the evolving contributions of gas transport, cracks and chemical kinetics during atmospheric carbonation of hydrated C3S and CSH pastes. *Cement and Concrete Research*, 160, 106906.
- Seigneur, N., Kangni-Foli, E., Lagneau, V., Dauzères, A., Poyet, S., & Le Bescop, P. (2020). L'Hôpital, E.; de Lacaillerie, J.-BD Predicting the atmospheric carbonation of cementitious materials using fully coupled two-phase reactive transport modelling. *Cem. Concr. Res*, 130, 105966.
- Seigneur, N., Lagneau, V., Corvisier, J., & Dauzères, A. (2018). Recoupling flow and chemistry in variably saturated reactive transport modelling-An algorithm to accurately couple the feedback of chemistry on water consumption, variable porosity and flow. *Advances in Water Resources*, 122, 355-366.
- Sellier, A., & Multon, S. (2018). Chemical modelling of Delayed Ettringite Formation for assessment of affected concrete structures. *Cement and Concrete Research*, 108, 72-86.
- Shen, W., Kondo, D., Dormieux, L., & Shao, J.-F. (2013). A closed-form three scale model for ductile rocks with a plastically compressible porous matrix. *Mechanics of Materials*, 59, 73-86.
- Shen, W., Shao, J.-F., Liu, Z., Oueslati, A., & De Saxcé, G. (2020). Evaluation and improvement of macroscopic yield criteria of porous media having a Drucker-Prager matrix. *International Journal of Plasticity*, 126, 102609.
- Socié, A., Seigneur, N., Bary, B., Poyet, S., & Touzé, G. (2023). A fully coupled Hydraulic Mechanical Chemical approach applied to cementitious material damage due to carbonation. *npj Materials Degradation*, 7(1), 60.
- Soler, J. M. (2022). *CI/CI-D Experiment: 3D Modeling for HTO and 36Cl. Reactive transport modeling of clay-concrete interaction*. Retrieved from
- Sukop, M. C., & Thorne, D. T. (2006). *Lattice Boltzmann Modeling*. Heidelberg: Springer Berlin.
- Thiery, M. (2005). *Modelling of atmospheric carbonation of cement based materials considering the kinetic effects and modifications of the microstructure and the hydric state*. Ecole des Ponts ParisTech,
- Tognazzi-Lawrence, C. (1998). *Couplage fissuration-dégradation chimique dans les matériaux cimentaires: caractérisation et modélisation*. Toulouse, INSA,
- van Breugel, K. (1995). Numerical simulation of hydration and microstructural development in hardening cement-based materials (I) theory. *Cement and Concrete Research*, 25(2), 319-331. doi:[https://doi.org/10.1016/0008-8846\(95\)00017-8](https://doi.org/10.1016/0008-8846(95)00017-8)
- Varzina, A., Cizer, Ö., Yu, L., Liu, S., Jacques, D., & Perko, J. (2020). A new concept for pore-scale precipitation-dissolution modelling in a lattice Boltzmann framework – Application to portlandite

carbonation. *Applied Geochemistry*, 123, 104786.
doi:<https://doi.org/10.1016/j.apgeochem.2020.104786>

- Vilarrasa, V., Makhnenko, R. Y., & Rutqvist, J. (2019). Field and laboratory studies of geomechanical response to the injection of CO₂. In *Science of carbon storage in deep saline formations* (pp. 209-236): Elsevier.
- von Greve-Dierfeld, S., Lothenbach, B., Vollpracht, A., Wu, B., Huet, B., Andrade, C., . . . Vanoutrive, H. (2020). Understanding the carbonation of concrete with supplementary cementitious materials: a critical review by RILEM TC 281-CCC. *Materials and structures*, 53(6), 136.
- Wu, J.-Y., & Chen, W.-X. (2022). On the phase-field modeling of fully coupled chemo-mechanical deterioration and fracture in calcium leached cementitious solids. *International Journal of Solids and Structures*, 238, 111380.